Three charged amino acids in extracellular loop 1 are involved in maintaining the outer pore architecture of CFTR

Guiying Cui,¹ Kazi S. Rahman,^{2,3} Daniel T. Infield,¹ Christopher Kuang,¹ Chengyu Z. Prince,¹ and Nael A. McCarty^{1,2}

¹Division of Pulmonary, Allergy and Immunology, Cystic Fibrosis, and Sleep, Department of Pediatrics, Center for Cystic Fibrosis and Airways Disease Research, Emory+Children's Pediatric Research Center, Emory University School of Medicine and Children's Healthcare of Atlanta, Atlanta, GA 30322

²Parker H. Petit Institute for Bioengineering and Bioscience and ³School of Biology, Georgia Institute of Technology, Atlanta, GA 30332

The cystic fibrosis (CF) transmembrane conductance regulator (CFTR) bears six extracellular loops (ECL1-6); ECL1 is the site of several mutations associated with CF. Mutation R117H has been reported to reduce current amplitude, whereas D110H, E116K, and R117C/L/P may impair channel stability. We hypothesized that these amino acids might not be directly involved in ion conduction and permeation but may contribute to stabilizing the outer vestibule architecture in CFTR. We used cRNA injected oocytes combined with electrophysiological techniques to test this hypothesis. Mutants bearing cysteine at these sites were not functionally modified by extracellular MTS reagents and were blocked by GlyH-101 similarly to WT-CFTR. These results suggest that these three residues do not contribute directly to permeation in CFTR. In contrast, mutants D110R-, E116R-, and R117A-CFTR exhibited instability of the open state and significantly shortened burst duration compared with WT-CFTR and failed to be locked into the open state by AMP-PNP (adenosine 5'-(β , γ -imido) triphosphate); charge-retaining mutants showed mainly the full open state with comparably longer open burst duration. These interactions suggest that these ECL1 residues might be involved in maintaining the outer pore architecture of CFTR. A CFTR homology model suggested that E116 interacts with R104 in both the closed and open states, D110 interacts with K892 in the fully closed state, and R117 interacts with E1126 in the open state. These interactions were confirmed experimentally. The results suggest that D110, E116, and R117 may contribute to stabilizing the architecture of the outer pore of CFTR by interactions with other charged residues.

INTRODUCTION

The Journal of General Physiology

The cystic fibrosis (CF) transmembrane conductance regulator (CFTR) is the only member of the ATP-binding cassette (ABC) transporter superfamily of proteins that behaves as a chloride ion channel. Mutations of CFTR directly cause the inherited disease CF; CFTR also plays an important role in polycystic kidney disease and secretory diarrhea (Gabriel et al., 1994; Sullivan et al., 1998). CFTR contains five functional domains. There are two distinct membrane-spanning domains (MSDs), each followed by a nucleotide-binding domain (NBD [NBD1 or NBD2]). These MSD-NBD pairs are linked by the regulatory domain (R), which is unique to CFTR and carries multiple PKA consensus sites (Hunt et al., 2013; Hwang and Kirk, 2013; Sebastian et al., 2013). Results from a broad range of approaches suggest that CFTR's ion channel pore has a relatively wide intracellular vestibule, a narrow central region, and a smaller extracellular vestibule

(Alexander et al., 2009; Cui et al., 2012; Norimatsu et al., 2012; Hwang and Kirk, 2013). Current models suggest that the two MSDs form an asymmetric channel pore (Bai et al., 2010; Gao et al., 2013; Hwang and Kirk, 2013). Each MSD includes six transmembrane (TM) helices; together, they contain six extracellular loops (ECLs) and four intracellular loops. The intracellular loops may be involved in dynamic regulation of CFTR channel gating, and recent data indicate that specific TM regions and ECLs contribute to the extracellular vestibule (Serohijos et al., 2008; Zhou et al., 2008). Although the TMs of CFTR, especially TM6 and TM12, have been studied extensively, the structure and function of the ECLs remain largely unknown (Cui et al., 2012). However, several known CFcausing mutations occur in the ECLs, indicating important structural and/or functional roles for these regions.

Four of CFTR's ECLs are very short with only a few amino acids in each; the remaining two, ECL1 and ECL4, are dramatically longer and have been shown to be

Correspondence to Nael A. McCarty: namccar@emory.edu

Abbreviations used in this paper: ABC, ATP-binding cassette; CF, cystic fibrosis; CFTR, CF transmembrane conductance regulator; DTT, dithiothreitol; ECL, extracellular loop; FRT, Fischer rat thyroid; ISO, isoproterenol; MSD, membrane-spanning domain; NBD, nucleotide-binding domain; TEVC, two-electrode voltage clamp; TM, transmembrane.

© 2014 Cui et al. This article is distributed under the terms of an Attribution–Noncommercial–Share Alike–No Mirror Sites license for the first six months after the publication date (see http://www.rupress.org/terms). After six months it is available under a Creative Commons License (Attribution–Noncommercial–Share Alike 3.0 Unported license, as described at http://creativecommons.org/licenses/by-nc-sa/3.0/).

important for CFTR stability and function. ECL4 bears the N-linked glycosylation site; absence of N-linked oligosaccharides in ECL4 reduces the stability of mature CFTR in the plasma membrane (Hanrahan et al., 1995; Glozman et al., 2009). CF-causing mutations have been identified in ECL1, including S108F, Y109C/N, D110H/Y/N, P111A/L, E116K/Q, and R117C/G/H/P/L. Among these residues, D110, E116, and R117 are charged amino acids fully conserved among nine species (Fig. 1 A). Mutations at each of these sites are associated with milder forms of CF; R117H in particular is associated with pancreatic sufficiency and is a common mutation related to mild CF (Kristidis et al., 1992; Sheppard et al., 1993).

Relatively little is known about the ECLs of CFTR; however, ECLs in many other channels have been found to be involved in channel gating, ion permeation, and drug effects. For example, the human acid-sensing ion channel 3 (ASIC3) exhibits intrinsic alkaline sensitivity through two arginines in an ECL (Delaunay et al., 2012). In the epithelial sodium channel (ENaC), ECL β9 in the palm domain and $\alpha 4$ in the thumb domain of the α subunit are in close proximity to the outer vestibule of the pore and are involved in the response to external stimuli such as external Na⁺ and sheer stress (Stockand et al., 2008; Shi et al., 2011). In addition, the ECL of the α subunit contains the binding site for the sulfonylurea drug glibenclamide, which activates ENaC (Renauld and Chraibi, 2009). In a small-conductance calcium-activated potassium channel, three amino acids in the S3-S4 ECL have been shown to be involved in apamin sensitivity and maintenance of pore shape (Weatherall et al., 2011). Finally, modulation of the voltage-dependent sodium channel

by the β-scorpion toxin (CssIV) is mediated by toxin binding to the ECLs of domains II and III, trapping the voltage sensor in its activated state (McPhee et al., 1998; Cestèle et al., 2006; Wang et al., 2011; Zhang et al., 2012).

Several lines of evidence indicate a role for the CFTR ECLs in modulating channel function. Sheppard et al. (1993) demonstrated that R117H exhibits reduced single-channel conductance, altered sensitivity to external pH, and altered single-channel kinetics resulting in reduction of macroscopic current. Using human-Xenopus laevis CFTR chimeras, Price et al. (1996) demonstrated that amino acid residues in ECL1 contribute to the gating of human CFTR. Hämmerle et al. (2001) reported that mutations D110H, E116K, and R117H induce no trafficking defect when expressed in baby hamster kidney (BHK) cells but affect channel function significantly. When studied in planar lipid bilayers, R117H-CFTR had gating kinetics similar to WT-CFTR, but a reduced single-channel conductance, whereas D110H- and E116K-CFTR displayed unstable channel openings, leading the authors to propose that ECL1 might contribute to maintaining the open pore architecture of CFTR (Hämmerle et al., 2001). In contrast, Zhou et al. (2008) proposed that R117 is located at the outmost part of the pore and acts to attract Cl⁻ ions into the CFTR pore, suggesting that R117 is involved in ion conduction and permeation via an electrostatic effect.

To gain a better understanding of the structure and function of the CFTR ECL1, we focused on its charged amino acids and endeavored to determine (a) whether they are directly involved in ion conduction and permeation, with mutations causing disease by reducing Cl⁻ flux;

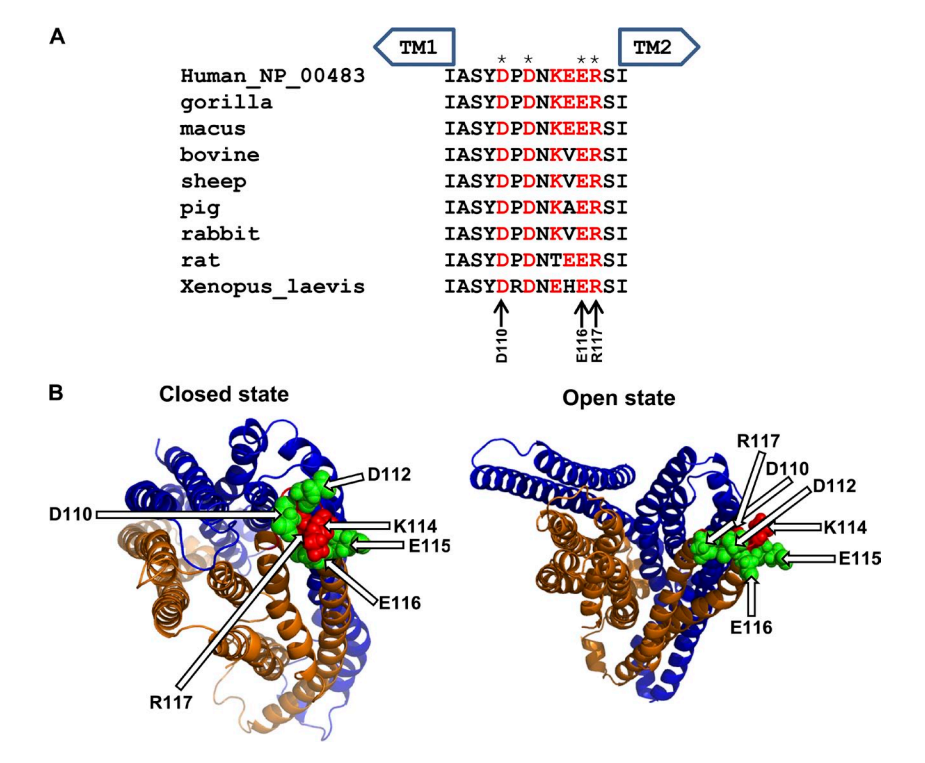


Figure 1. ECL1 sequence alignment and homology model. (A) Sequence alignment of ECL1 in CFTR proteins from nine species. Charged residues are indicated in red. Asterisks indicate residues conserved in multiple species. D110, E116, and R117 are diseaserelated and conserved residues labeled with arrows. (B) Top view of the homology model of CFTR (McCarty laboratory model; Rahman et al., 2013) with charged acidic (green) and basic (red) amino acids shown as spheres; model prepared with PyMOL. (left) Closed state (equivalent to the state where the NBDs are fully dedimerized). (right) Open state. TM1-6 is indicated in brown shades, and TM7-12 is indicated in blue shades.

(b) whether and how they contribute to maintaining open pore architecture; and (c) whether ECL1 moves during the CFTR gating cycle. We have combined molecular biology and electrophysiological techniques guided by our new homology model (Rahman et al., 2013) to probe these questions. Our results identify possible functions of ECL1 in human CFTR.

MATERIALS AND METHODS

Preparation of oocytes and cRNA

The mutants used in this study were prepared using site-directed mutagenesis with the QuikChange protocol (Agilent Technologies). All cRNAs for electrophysiology experiments were prepared from constructs encoding WT-CFTR in the pGEMHE vector, which was provided by D. Gadsby (The Rockefeller University, New York, NY). All mutant constructs were verified by sequencing across the entire open reading frame before use. *Xenopus* oocytes were injected in a range of 1–10 ng CFTR cRNAs and were incubated at 18°C in modified Leibovitz's L-15 media with the addition of HEPES, pH 7.5, penicillin, and streptomycin. Recordings were made 24–72 h after the injection of cRNAs. Methods of animal handling are in accordance with the National Institutes of Health guidelines, and the protocol was approved by the Institutional Animal Care and Use Committee of Emory University.

Electrophysiology

For single-channel recording, CFTR channels were studied in excised, inside-out patches at room temperature (22-23°C; McCarty et al., 1993; Fuller et al., 2007). Oocytes were prepared for study by shrinking in hypertonic solution (mM: 200 monopotassium aspartate, 20 KCl, 1 MgCl₂, 10 EGTA, and 10 HEPES, pH 7.2 adjusted with KOH), followed by manual removal of the vitelline membrane. Pipettes were pulled from borosilicate glass (Sutter Instrument) and had resistances averaging ${\sim}10~\text{M}\Omega$ when filled with chloride-containing pipette solution (mM): 150 NMDG-Cl, 5 MgCl₂, and 10 TES, pH 7.5. The reducing agent dithiothreitol (DTT) was dissolved in DMSO to 1 M as stock solution (stored at −20°C) and diluted to a final concentration of 1 mM with pipette solution and directly filled or backfilled into the pipette, depending on the experimental goal. Typical seal resistances were 200 G Ω or greater. Channels were activated by excision into intracellular solution containing (mM) 150 NMDG-Cl, 1.1 MgCl₂, 2 Tris-EGTA, 10 TES, 1 MgATP, and 50 U/ml PKA, pH 7.5. CFTR currents were measured with an Axopatch 200B amplifier (Molecular Devices) and were recorded at 10 kHz to DAT tape. For subsequent analysis, records were played back and filtered with a four-pole Bessel filter (Warner Instruments) at a corner frequency of 1 kHz and acquired using a Digidata 1322A interface and computer at 500 Hz with pCLAMP 8.2 (Molecular Devices). For display, single-channel records were filtered digitally to 100 Hz. pCLAMP version 10.2 was used to analyze single-channel current and to make all-points amplitude histograms, which had a bin width of 0.01 pA and were fit with Gaussian distributions using Clampfit 10.2. Window current (calculated as the rolling mean of current in a 1-min window, in pA) over each minute for WT- and D110C/K892C-CFTR records was measured sequentially for 21 min with Clampfit 10.2. The open duration analysis was performed on records from patches containing one to three active CFTR channels as previously described (Fuller et al., 2005). Open duration histograms were made and fit with a single exponential function with Igor version 4.01 (WaveMetrics). Apparent open probability (NP_o) was measured using Clampfit 10.2. Opening rates for WT- and R104C/ E116C-CFTR were measured as previously described except that

only records containing one to three active channels per patch were analyzed (Wang et al., 2005).

For inside-out macropatch recording, patch pipette resistances were 1–2 $M\Omega$ and the same symmetrical 150 mM Cl $^-$ solutions were used as for single-channel recording. Macropatch recordings were performed with an Axopatch 200B amplifier operated by pCLAMP 8.2 software, filtered at 100 Hz with a four-pole Bessel filter and acquired at 2 kHz. After forming an inside-out macropatch, a voltage ramp protocol was applied every 5 s, holding at $V_M=0$ mV then stepping up to 100 mV for 50 ms, followed by a ramp down to -100 mV over 300 ms and then a step back to 0 mV.

Standard two-electrode voltage clamp (TEVC) techniques were used to study MTS reagent-induced modification of introduced cysteines and the blocking effects of GlyH-101 on WT-CFTR and mutants, with application of reagents to the extracellular side. Each oocyte was injected with CFTR cRNA along with cRNA encoding the β_2 -adrenergic receptor (McDonough et al., 1994; McCarty and Zhang, 2001). Pipette resistances measured 0.5–1.4 M Ω when filled with 3 M KCl and measured in standard ND96 bath solution that contained (mM) 96 NaCl, 2 KCl, 1 MgCl $_2$, and 5 HEPES, pH 7.5. CFTR channels were activated by exposure to 10 μ M isoproterenol (ISO) alone and alternatively assayed in the presence of DTT, MTS reagents, or GlyH-101 in the bath solution. Currents were acquired with an Axoclamp 900A amplifier and Clampex 10.2 software, and current data were digitized at 2 kHz.

Fractional change of current (F_c) at steady-state in response to exposure to drugs or chemicals was calculated according to the equation

$$F_c = 1 - I_b / I_c$$

where I_c and I_b represent the steady-state control currents and currents in the presence of chemicals (GlyH-101 or MTS reagents), respectively.

Macroscopic current-voltage relationships were recorded with an I-V slope protocol, holding at $V_{\rm M}=0$ mV, step to -100 mV for 50 ms, ramp to 100 mV over 250 ms, and step to 0 mV. Background currents were recorded before ISO and subtracted before further analysis. Reversal potentials were determined by linear regression around the zero-current value. Rectification ratio was quantified with the following equation:

Rectification ratio =
$$|\mathbf{I}|_{(80\text{mV})} / |\mathbf{I}|_{(-80\text{mV})}$$
,

where $|I|_{(80mV)}$ is the absolute value of current at $V_{\rm M}$ = 80 mV and $|I|_{(-80mV)}$ is the absolute value of current at $V_{\rm M}$ = -80 mV.

Source of reagents

Unless otherwise noted, all reagents were obtained from Sigma-Aldrich. L-15 media was from Gibco. GlyH-101 was from EMD Millipore. All MTS reagents were from Toronto Research Chemicals Inc. PKA was from Promega. GlyH-101 was prepared as a stock solution at 50 mM in DMSO. MTS reagents were prepared as a stock solution at 0.1 M in DMSO or $\rm H_2O$ and diluted to a final concentration of 1 mM immediately before use.

Statistics

Unless noted, values given are mean \pm SEM. Statistical analysis was performed using the t test for unpaired or paired measurements by Sigma Stat 2.03 (Jandel Scientific), with P < 0.05 considered indicative of significance. *, P < 0.05; **, P < 0.01; $^{\#}$, P < 0.001.

Online supplemental material

Fig. S1 illustrates representative single-channel current traces of D110R-, E116R-, and R117A-CFTR with a larger time scale

compared with Fig. 2 A. Fig. S2 shows the voltage-dependent and concentration-dependent effects of GlyH-101 (GlyH) on WT-CFTR. Fig. S3 shows representative I-V curves of D110R-, E116R-, and R117A-CFTR recorded in symmetrical 150 mM Cl⁻ solution with the inside-out macropatch technique. Fig. S4 illustrates characteristics of multiple possible salt bridge partners for D110, E116, and R117, including E217, D891, R899, R104, and E1124. Fig. S5 illustrates representative single-channel current traces of E116R/ K892E- and R104E/D110R-CFTR and their mean burst durations. Fig. S6 shows representative I-V plots of double mutants R104E/ E116R- and R117E/E1126R-CFTR and their rectification ratio. Fig. S7 shows representative TEVC current traces of WT- and D110C/ K892C-CFTR with DTT pretreatment. Fig. S8 illustrates a schematic model of CFTR channel gating and two views of the 2.5-ns snapshot along the CFTR homology model simulation. Online supplemental material is available at http://www.jgp.org/cgi/ content/full/jgp.201311122/DC1.

RESULTS

Mutations at three charged amino acids in ECL1 reduce burst stability and burst duration

The six charged amino acids in ECL1 of human CFTR are widely conserved among nine species, including four that are completely conserved (Fig. 1 A). Three of these, D110, E116, and R117, are the sites of known CFrelated mutations. To probe the potential mechanisms by which mutation of these charged residues leads to CF, we first recorded the single-channel behavior of a series of CFTR channel mutants bearing a single mutation at one of the six charged sites (D110R, D112R, K114D, E115R, E116R, or R117A). Recordings were made in inside-out patches from Xenopus oocytes injected with WT or mutant CFTR cRNA. Representative currents and all-points amplitude histograms for single-channel currents recorded at $V_M = -100$ mV are shown in Fig. 2 A. The single-channel amplitudes of the six mutants varied, but all were significantly different from WT-CFTR (Fig. 2 B). No current was detected in either inside-out patch or TEVC recording from oocytes expressing R117E-CFTR; therefore, it was not studied further.

Unlike WT-CFTR, which opens mainly to the full open state (f) with subconductance states as rare events, D110R-, E116R-, and R117A-CFTR exhibited multiple open states, including subconductance state 1 (s1), subconductance state 2 (s2), and the f state (Fig. S1). This is similar to our previous findings for TM6 mutants R334C-, R352A-, R347C/H-CFTR (Cotten and Welsh, 1999; Zhang et al., 2005b; Cui et al., 2008). Mean burst durations for these mutants were drastically shorter than for WT-CFTR (P < 0.001; Fig. 2 C). In contrast, D112R- and E115R-CFTR each mainly opened to the full open state with subconductance states appearing as rare events and mean burst durations very close to that of WT-CFTR. The exception was K114D-CFTR, which exhibited mean burst duration significantly shorter than that of WT-CFTR, but much longer than that of D110R-, E116R-, and R117A-CFTR. The apparent open probabilities of D110R-, E116R-, and R117A-CFTR were significantly lower than WT-CFTR (Fig. 2 D). Because K114 has not been identified as a CF disease–related amino acid so far, we focused on D110, E116, and R117 in the rest of this work.

It is well known that AMP-PNP (adenosine 5'- $(\beta, \gamma$ imido) triphosphate), a nonhydrolyzable ATP analogue, binds to the NBD domains of CFTR to lock the channel into a prolonged full open state. AMP-PNP also locks mutant R334C-CFTR into a long stable s2 state (Fuller et al., 2005; Zhang et al., 2005b). Given the instability of D110R-, E116R-, and R117A-CFTR single-channel openings, we asked whether AMP-PNP would lock these mutants into a stable open state. As, expected, addition of 2.75 mM AMP-PNP in the presence of 1 mM MgATP and PKA more than doubled the mean burst duration for WT-CFTR, from 683 ms in the absence of AMP-PNP (n = 6) to 1,579 ms (n = 3). In contrast, AMP-PNP did not affect mean burst duration or single-channel amplitude of R117A-CFTR but did increase the apparent open probability (P < 0.05; Fig. 3). Similar results were seen in D110R- and E116R-CFTR (mean burst duration for E116R: -AMP-PNP, 37.72 ± 3.07 ms; +AMP-PNP, 36.16 ± 5.73 ms, n = 3; and for D110R-CFTR: -AMP-PNP, 22.24 ± 1.8 ms; +AMP-PNP, 19.74 ± 0.69 ms, n = 4). Hence, burst duration was not increased by AMP-PNP in these ECL1 mutants, nor did it rescue their flickery open channel behavior. These data suggest that the altered behavior in the mutants may be caused by loss of a local interaction in the pore (i.e., "pore gating"), as proposed previously by our group (Cui et al., 2013).

MTS reagents do not modify ECL1 mutant function

Substituted cysteine accessibility methods have been used to identify pore-lining residues in the TMs of CFTR as well as to test structure-function relationships in numerous other transporters and channels (Liu et al., 2001; DeCaen et al., 2008). If D110, E116, and R117 directly contribute to ion conduction and permeation in CFTR via an electrostatic effect, the macroscopic current amplitudes of mutants bearing cysteines engineered at these sites should be changed by covalent modification with charged, membrane-impermeant MTS reagents. Therefore, we performed experiments to investigate the modification of WT-, D110C-, E116C-, and R117C-CFTR by MTSET (ET⁺) and MTSES (ES⁻) with the TEVC technique; R334C-CFTR was used as a positive control (Zhang et al., 2005b). Oocytes were held at a membrane potential of -60 mV, while CFTR channels were activated with 10 µM ISO in ND96 solution (Fig. 4). When CFTR current reached a plateau, 10 µM ISO with 1 mM ET⁺ or ES⁻ was washed on for 1 min. As in our previous work (Zhang et al., 2005b), neither ET⁺ nor ES⁻ caused detectable functional modification of WT-CFTR when applied to the extracellular side. In contrast, both ET⁺ and ES induced functional covalent modification of R334C-CFTR: ET⁺ increased macroscopic current by 39%

(fractional change = 0.39 ± 0.05), and ES⁻ decreased it by 30% (fractional change = -0.30 ± 0.04 ; Fig. 4), indicating that modification gave rise to changes in anion conduction (Zhang et al., 2005b). However, under the same conditions, no functional modifications were observed for any of the three ECL1 cysteine mutants studied (D110C-, E116C-, and R117C-CFTR). These data differ from those of Zhou et al. (2008) who reported that R117C-CFTR could be modified by both ET⁺ and ES⁻. This difference probably arises from differences in experimental design. Zhou et al. (2008) preincubated cells expressing R117C-CFTR in solution with ET⁺ or ES⁻ before the experiment and compared the data with a group of unexposed cells, whereas we investigated the effects of modification in real time and compared data before and after exposure to the reagents in the same oocytes. Our data could be interpreted in two ways: (1) the thiol groups of the engineered cysteines in D110C-, E116C-, and R117C-CFTR were not exposed and therefore unable to be modified by ET⁺ or ES⁻, or (2) the three cysteines

in these positions were modified by ET⁺ and ES⁻, but their modification failed to affect ion conduction because these amino acids are located too far away from the Cl⁻ conduction pathway. In either case, our results suggest that none of these residues contributes directly to ion conduction through the CFTR channel.

ECL1 mutations have no effect on CFTR blockade by the open pore blocker GlyH-101

GlyH-101 is the first open pore blocker of human CFTR that functions from the extracellular side (Muanprasat et al., 2004). The negatively charged GlyH-101 blocked WT-CFTR current recorded from Fischer rat thyroid (FRT) cells with an IC₅₀ of 1.4 μ M at V_M = 60 mV and 5.6 μ M at V_M = -60 mV (Muanprasat et al., 2004). Although GlyH-101 has been proposed to bind to a site near position T338 in the narrow part of the CFTR pore, consistent with its strong voltage dependence, it is unclear whether other parts of CFTR are involved in blockade by GlyH-101 (Norimatsu et al., 2012). We hypothesized

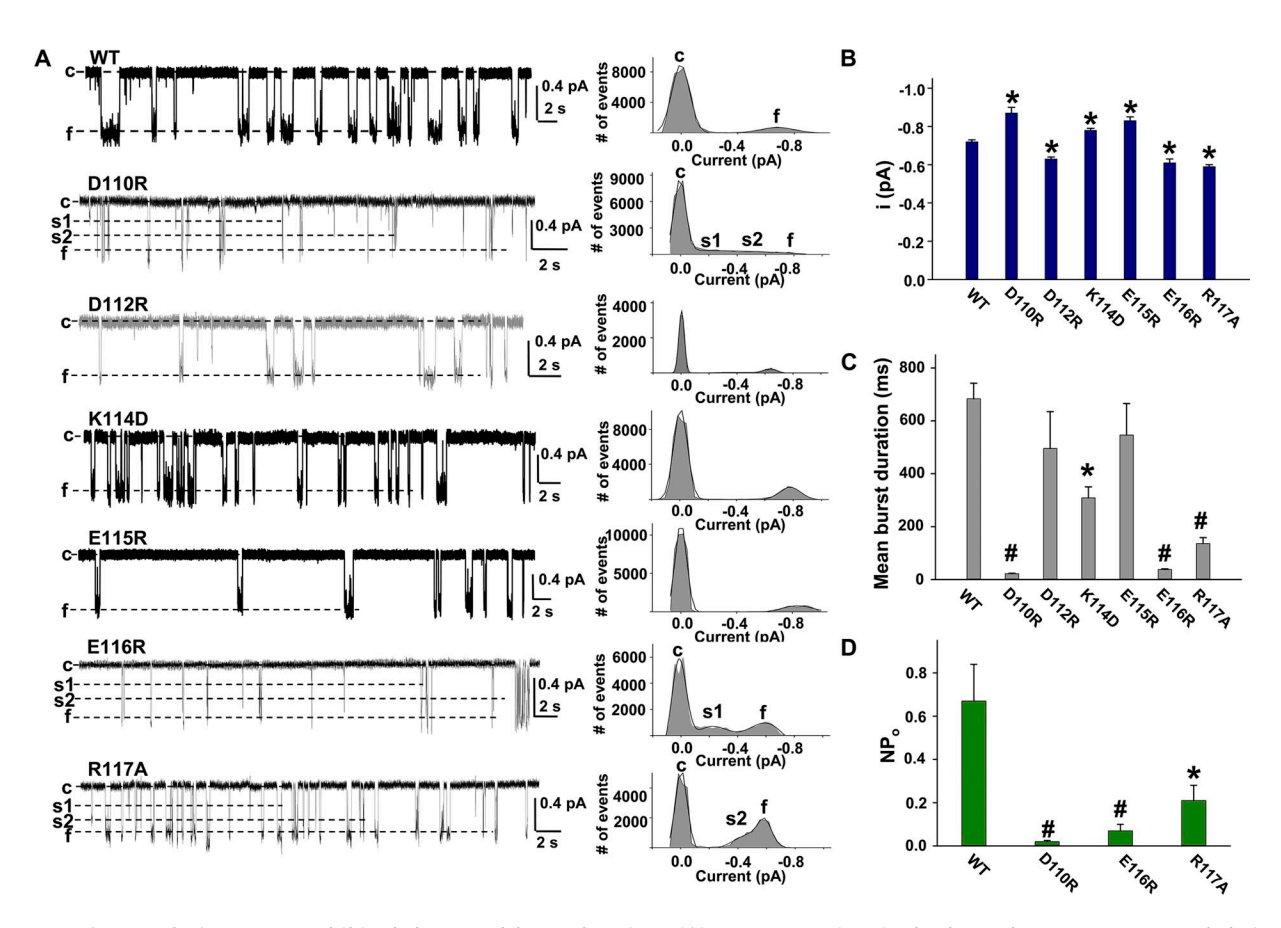


Figure 2. Some ECL1 mutants exhibited decreased burst duration. (A) Representative single-channel current traces and their all-points histograms for WT-, D110R-, D112R-, K114D-, E115R-, E116R-, and R117A-CFTR from inside-out membrane patches excised from *Xenopus* oocytes, with symmetrical 150 mM Cl⁻ solution in the presence of 1 mM MgATP and 50 U/ml PKA. All traces were recorded at $V_{\rm M} = -100$ mV. c, closed state; f, full open state; s1 and s2, subconductance states 1 and 2. The solid lines in the histograms are fit results to a Gaussian function. (B and C) Single-channel amplitudes of the full open state (B) and mean burst durations (C) of WT-, D110R-, D112R-, K114D-, E115R-, E116R-, and R117A-CFTR. (D) Apparent open probability of WT-, D110R-, E116R-, and R117A-CFTR. *, P < 0.05 compared with WT-CFTR; #, P < 0.001 compared with WT-CFTR. n = 4-7 for all variants. Mean ± SEM is shown. This analysis reflected only openings to the f state.

that the charged amino acids in ECL1 might be involved in establishing the appropriate architecture for GlyH-101 binding and function. To test this hypothesis, we first used the TEVC technique to establish whether GlyH-101 blocked WT-CFTR expressed in *Xenopus* oocytes with similar concentration and voltage dependence as CFTR expressed in FRT cells. Representative current traces are shown in Fig. S2 (A and B). These results indicate that GlyH-101 blocked WT-CFTR channels expressed in oocytes with similar efficacy as in FRT cells (Muanprasat et al., 2004). When oocytes were held at $V_{\rm M}$ = -30 mV and stepped up to 80 mV for 75 ms, GlyH-101 blocked WT-CFTR current in a concentrationdependent manner with $K_d = 0.98 \mu M$. To test whether GlyH-101 blocks CFTR steady-state currents, oocytes were held at $V_M = -60$ mV and CFTR channels were activated by 10 μM ISO. In these cells, GlyH-101 added once current plateaued reversibly blocked CFTR-mediated current $(K_d = 4.9 \,\mu\text{M})$. Representative current traces and summary data are shown in Fig. 5. Under these conditions, 2.5 µM GlyH-101 blocked WT-CFTR, reducing current by $28 \pm 3\%$. GlyH-101 blocked D110C- and R117C-CFTR similarly to WT-CFTR, whereas E116C-CFTR was also blocked significantly by GlyH-101 (P < 0.01), but less efficaciously than the other two mutants or the WT. These data suggest that ECL1 amino acids D110, E116, and R117 do not contribute to the binding sites for GlyH-101 and are not directly involved in GlyH-101-mediated inhibition.

ECL1 mutations shift the reversal potential in macroscopic currents

To further verify that these ECL1 amino acids do not strongly or directly affect ion conduction and permeation, we compared the reversal potentials (V_{rev}) of D110R-, K114D-, E116R-, and R117A-CFTR with WT-CFTR and with the R334A mutant, which has been shown to have a profound effect on V_{rev} compared with WT-CFTR, consistent with the role of R334 in providing charge in the outer mouth of the open channel. Recordings were made in ND96 solution; representative currents are shown in Fig. 6 and summary data are shown in Table 1. E116Rand R117A-CFTR exhibited significantly right-shifted reversal potentials compared with WT-CFTR, but the effects were not as large as for R334A-CFTR. In contrast, neither D110R- nor K114D-CFTR altered V_{rev}. We also determined the rectification ratio for each mutant (see Materials and methods) and compared it with WT-CFTR, which had a rectification ratio of 2.10 ± 0.09 (n = 20). As previously reported, R334A-CFTR exhibited outward rectification but with a significantly reduced rectification ratio: 1.33 ± 0.14 (n = 9, P < 0.01). Of the ECL1 mutants we examined, the rectification ratios for D110R-, K114D-, and R117A-CFTR were similar to WT-CFTR (Fig. 6), whereas E116R-CFTR showed significantly reduced outward rectification. We also examined the I-V relationship of D110R-, E116R-, and R117A-CFTR with the inside-out macropatch technique in symmetrical

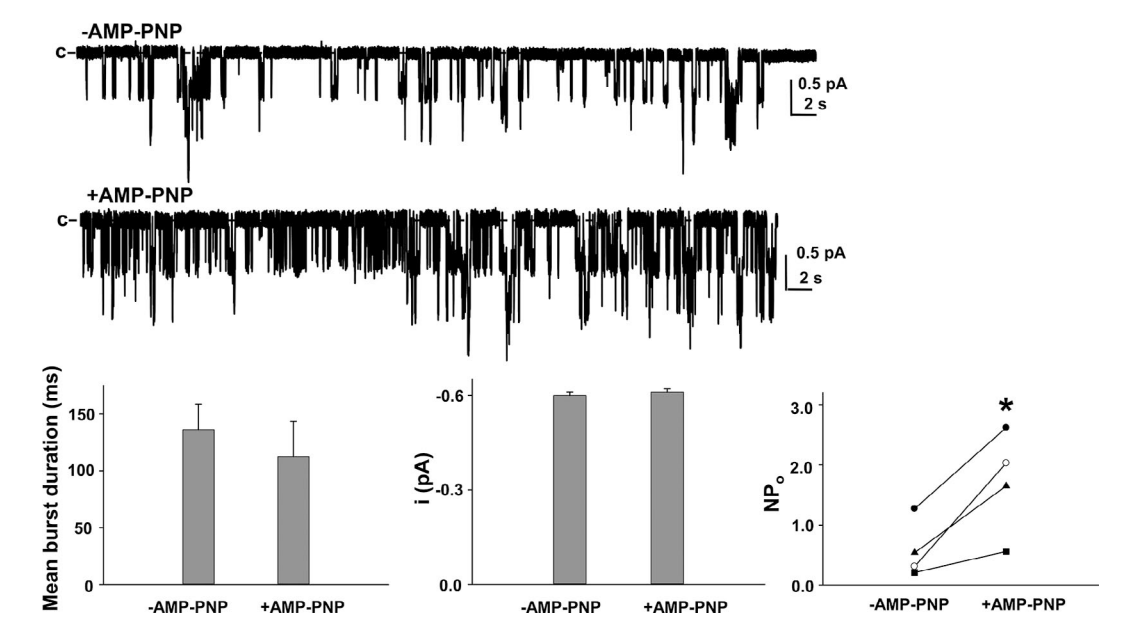


Figure 3. R117A-CFTR failed to be locked into a stable open state by AMP-PNP. R117A-CFTR was activated with 1 mM Mg-ATP and PKA and recorded under control conditions with ATP + PKA (-AMP-PNP), followed by addition of 2.75 mM AMP-PNP (+AMP-PNP). Representative traces shown were recorded from the same patch at $V_M = -100$ mV. The bottom panel shows mean burst duration for openings to the full conductance state (left), single-channel amplitude (middle), and apparent open probability (NP $_0$; right). AMP-PNP had no effect on mean burst duration or single-channel amplitude but significantly increased apparent open probability of R117A-CFTR (n = 4). *, P < 0.05 compared with ATP and PKA alone (-AMP-PNP). Mean \pm SEM is shown.

150 mM Cl⁻ solution; representative data are shown in Fig. S3. Under these conditions, E116R-CFTR exhibited slight inward rectification, but both D110R- and R117A-CFTR exhibited linear I-V relationships like that of WT-CFTR. The data again supported the conclusion that ECL1 amino acids are not directly involved in attracting Cl⁻ into the CFTR pore.

The data presented so far resolve our first two questions in this paper: (1) Charge-swapping mutations of D110, E116, and R117 of ECL1 destabilize the open state, indicating that these residues contribute to maintaining the outer mouth open pore architecture of CFTR; (2) based

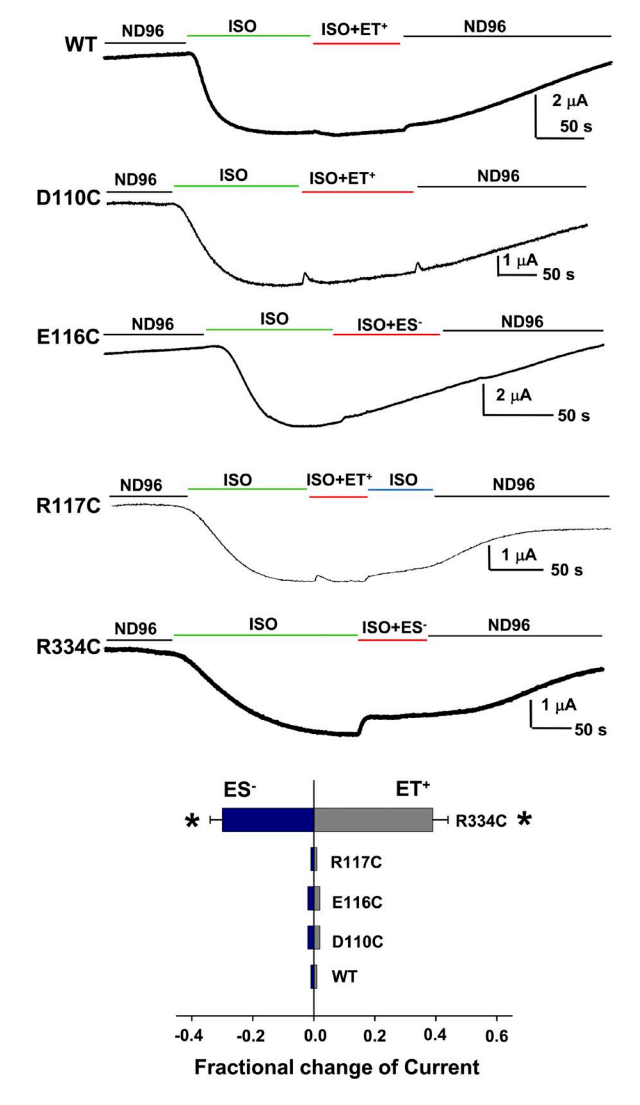


Figure 4. Effects of 1 mM MTSET+ (ET+) and MTSES- (ES-) on WT-, D110C-, E116C-, R117C-, and R334C-CFTR. Representative whole-cell TEVC current traces were recorded at $V_{\rm M}=-60$ mV in ND96 solution in cells expressing CFTR with the β_2AR (see Materials and methods). After activation with 10 μM ISO, oocytes were exposed to 1 mM ET+ or ES- in the continuing presence of ISO. Summary data for all mutants tested under the same conditions are shown below the sample current traces. Some error bars are too small to view. *, P < 0.05 compared with WT-CFTR. n=4–6. Mean \pm SEM is shown.

on the effects of ECL1 mutations on single-channel amplitudes, GlyH-101 blocking effects, reversal potentials, and rectification ratios and the effects of amino acid modification by MTS, we conclude that ECL1 is not directly involved in ion conduction and permeation in CFTR.

Charge-retaining substitutions at D110, E116, and R117 partially rescue the stability of open bursts

Because our data strongly suggest that D110, E116, and R117 in ECL1 are mainly involved in maintaining a stable open state, we explored the underlying mechanism. We first asked whether charge-retaining substitutions at D110, E116, and R117 would recover the stability of the open burst in CFTR. We generated D110E-, E116D-, and R117K-CFTR and observed their single-channel behavior with the inside-out patch technique in symmetrical 150 mM Cl $^-$ solution at $V_{\rm M}=-100$ mV. Sample currents are shown in Fig. 7 (A–C). D110E-CFTR exhibited a much more stable full open state with mean burst duration significantly longer than D110R-CFTR (P < 0.001; Fig. 7, A and E). Similar results were observed when the burst durations of E116D-CFTR and E116R-CFTR were compared (P < 0.001; Fig. 7, B and E). However, this effect

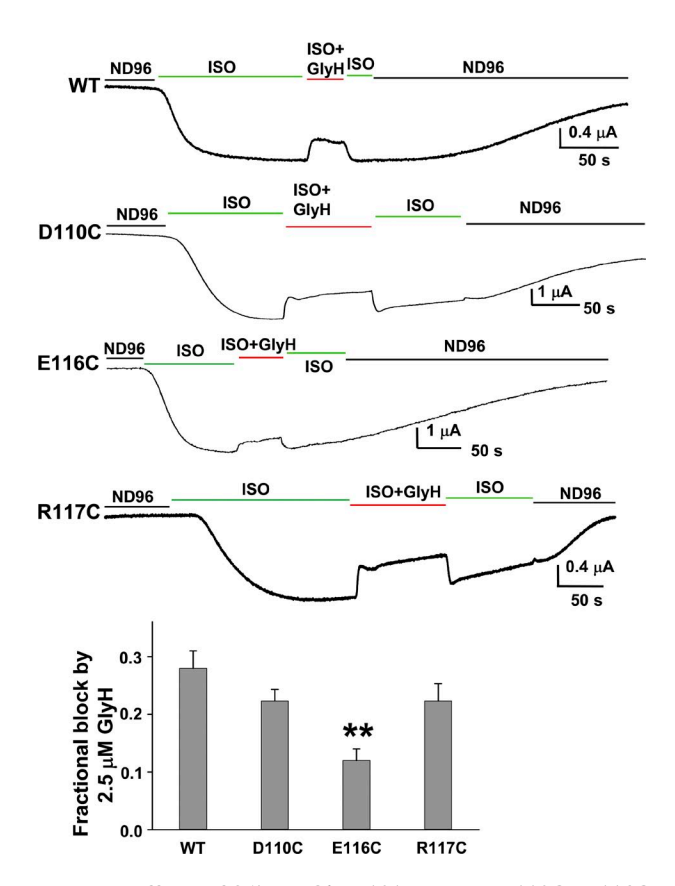


Figure 5. Effects of 2.5 μ M GlyH-101 on WT-, D110C-, E116C-, and R117C-CFTR. Representative current traces recorded from CFTR expressed in oocytes, at $V_{\rm M}=-60$ mV. Fractional block of WT-CFTR and mutants with 2.5 μ M GlyH is shown below the current traces. **, P < 0.01 compared with WT-CFTR. n=5–8. Mean \pm SEM is shown.

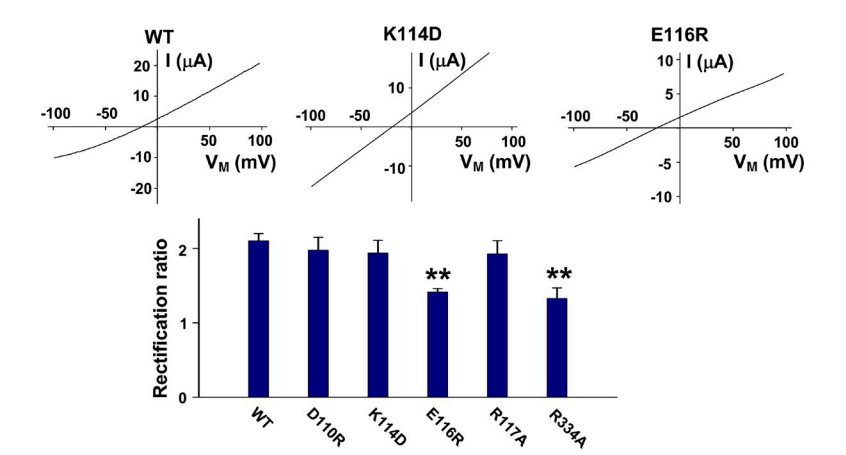


Figure 6. Some ECL1 mutants exhibit altered rectification. WT-CFTR, K114D-CFTR, and E116R-CFTR currents were generated under a voltage protocol wherein membrane potential was held at 0 mV for 50 ms then ramped from -100 mV to 100 mV over 300 ms with the TEVC technique. Standard ND96 was used as bath solution. Currents are shown after subtraction of background currents (in the absence of $10 \,\mu\text{M}$ ISO). Rectification of the I-V relationship (rectification ratio) was quantified as defined in Materials and methods. **, P < 0.01 compared with WT-CFTR. n = 5-7. Mean \pm SEM is shown.

was less marked when R117K- and R117A-CFTR were compared (P < 0.05; Fig. 7, C and E). Although the charge-conserving mutations improved burst durations, they only partially recovered the duration of WT-CFTR bursts. Single-channel amplitudes of these mutants were only slightly different from WT-CFTR regardless of their charge, suggesting again that the three charged amino acids are not involved in electrostatic interactions with Cl⁻ ions (Fig. 7 D). These data indicate that charge-retaining mutations at D110, E116, and R117 at least partially rescued the stability of the open pore, probably by maintaining the outer mouth open architecture of CFTR. In addition, the fact that charge retaining mutants only confer partial rescue suggests that side-chain orientation is specific in the WT channel.

D110, E116, and R117 do not interact with each other locally Because charge-retaining ECL1 amino acid mutations D110E, E116D, and R117K partially rescued a steady

TABLE 1
Reversal potentials of WT-CFTR and mutants in ND96 bath solution

CFTR	n	$ m V_{rev}$
		mV
WT	14	-27.75 ± 0.78
R334A	6	-12.15 ± 1.64^{a}
R117A	6	-22.51 ± 0.85^{a}
E116R	5	-21.45 ± 1.14^{a}
K114D	5	-24.68 ± 3.22
D110R	5	-27.64 ± 3.29
R104E	5	-21.15 ± 1.08^{a}
R899C	4	-25.30 ± 3.94
D891C	6	-25.81 ± 2.44
K892E	5	-23.70 ± 3.62
E1124R	5	-18.32 ± 0.43^{a}
E1126R	5	-20.67 ± 3.16^{b}
R117E/E1126R	6	-23.06 ± 1.37^{b}
R104E/E116R	6	-27.17 ± 1.08

Values are mean \pm SEM. n, number of oocytes. V_{rev} , reversal potential for Cl^-

open state, we hypothesized that these residues might interact with other amino acids in ECL1 to form salt bridges. D110, E116, and R117 reside in an unstructured loop which, unlike an α helix or β strand, is generally unstable and could require fine tuning to maintain its architecture. Thus, local interactions between amino acids might hold ECL1 in the correct position during the channel gating cycle. To test this hypothesis, we first made the mutants E116R/R117E-, D110R/R117E-, and D110R/E116R/R117E-CFTR and studied their singlechannel properties. Representative currents are shown in Fig. 8. All three mutants exhibited very brief openings to the s1, s2, and f states, with mean burst durations significantly lower than that of WT-CFTR (P < 0.001; Fig. 8 B) and R117A-CFTR (Fig. 2 C), but not different from D110R-CFTR and E116R-CFTR (Fig. 2 C). These data suggest that the three charged amino acids in ECL1 do not interact with each other locally to fulfill their function. In addition, the fact that the double and triple mutants showed single-channel amplitude only slightly different from WT-CFTR further supports the notion that these residues are not critical for attracting Cl⁻ ions into the CFTR channel outer pore (Fig. 8 C).

Identification and characterization of possible salt bridge partners for D110, E116, and R117

To identify amino acid residues in other regions that might interact with D110, E116, and R117, we performed a global search for positively and negatively charged amino acids in the extracellular face of CFTR, which might form salt bridges with these residues based on the available CFTR homology models (Mornon et al., 2008, 2009; Serohijos et al., 2008; Alexander et al., 2009). This identified several possible candidates including E217 (TM3), D891 (ECL4), R899 (ECL4), and E1124 (ECL6). We characterized CFTR with mutations at each of these sites to assess the likelihood of interaction with the charged ECL1 residues (Fig. S4). If the functional roles of D110, E116, or R117 are dependent on interaction with another amino acid in CFTR, we would expect mutation of either partner amino acid to have similar functional effects.

 $^{^{\}mathrm{a}}\mathrm{P} < 0.001$ compared with WT-CFTR by t test.

 $^{^{\}rm b}$ P < 0.01 compared with WT by t test.

Instead, we found that mutations at E217, D891, R899, or E1124 had no significant effect on single-channel behavior (Fig. S4 A, bottom). We did not observe any evidence of covalent modification of E1124C-, D891C-, or R899C-CFTR; there was no change in current upon exposure to either MTSET⁺ or MTSES⁻. E1124C-CFTR current was transiently increased by MTSET⁺, but in a noncovalent manner (Fig. S4 B). Mutants D891C- and E1124R-CFTR exhibited slight changes in rectification compared with WT-CFTR (Fig. S4 C), and reversal potentials were also similar to that of WT-CFTR; the reversal potential of E1124R-CFTR was shifted toward zero (Table 1). R899 was previously identified as a Cl⁻-binding site that might help to attract ions into the CFTR pore (El Hiani and Linsdell, 2012; Li et al., 2012). However, in our hands, the R899C mutation had no effect on channel function. E217 has recently been suggested to form a salt bridge with R334 when CFTR is in the closed state (Rahman et al., 2013). These data indicate that none of the candidates we tested based on predictions of earlier homology models are likely interaction partners with the three ECL1 amino acids under study.

Our recently published new CFTR homology model and its molecular dynamic simulation predicted additional salt bridge partner candidates: R104, K892, and E1126 (Rahman et al., 2013). R104 (TM1) may form a salt bridge with E116 in the closed state and the bridge may persist in the open state. K892 (ECL4) was predicted to form a salt bridge with D110 in the closed state (Rahman et al., 2013). E1126 (ECL6) was proposed to be a candidate for interaction with R117 in the open state.

E116 forms a salt bridge with R104 in the open state as well as in the closed state

To test the above prediction that R104 is a partner for E116, we studied the single mutant R104E-CFTR and the charge-swap double mutants R104E/E116R- and R104E/D110R-CFTR. R104 is proposed to sit in the mouth of the CFTR pore at the extracellular end of TM1. Both R104E-CFTR and R104E/E116R-CFTR exhibited reduced outward rectification with similar reversal potentials, both significantly different from WT-CFTR (Figs. S4 C and S6 and Table 1). Single-channel recording of R104E-CFTR (representative trace in Fig. 9 A) revealed

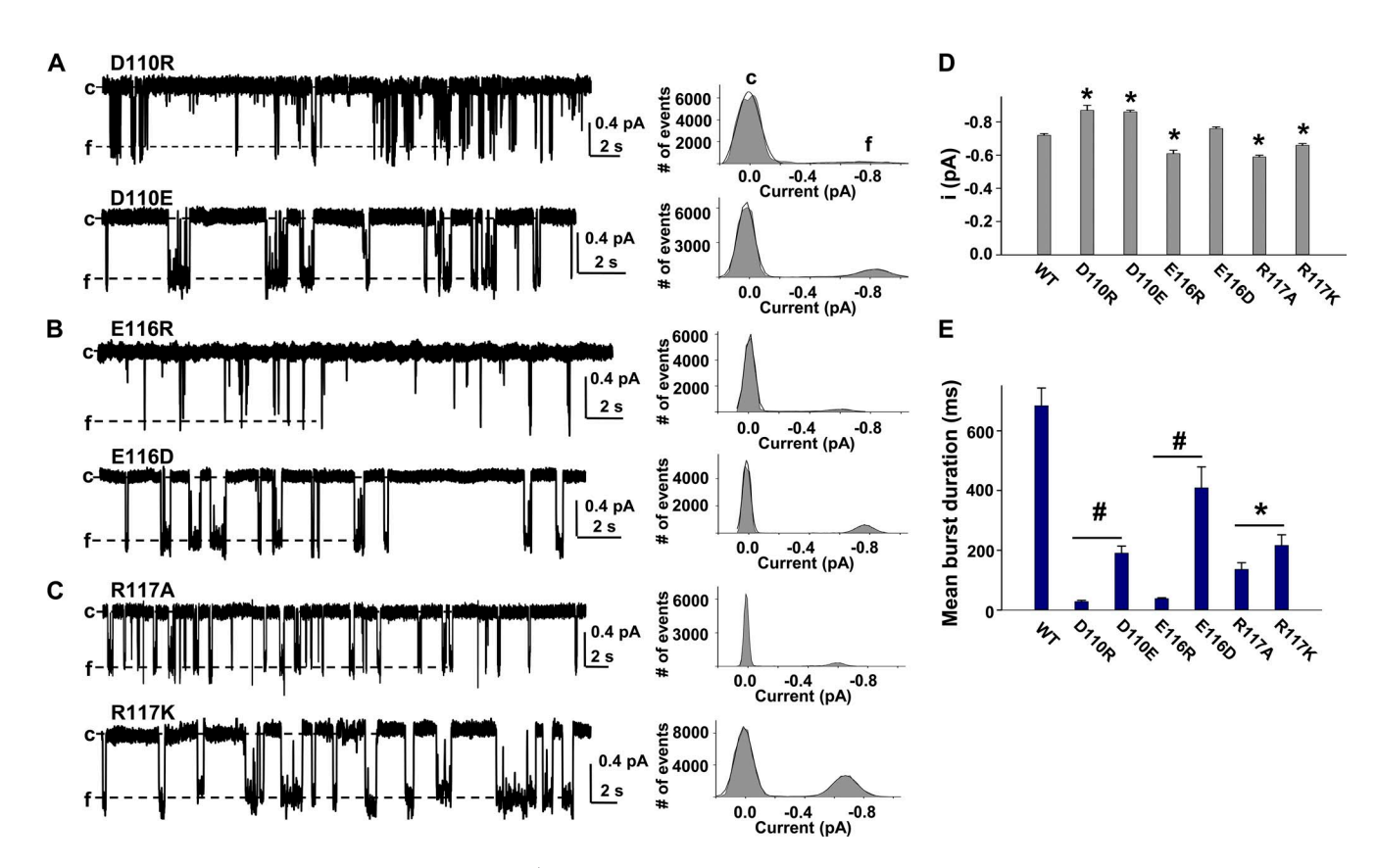


Figure 7. Charge recovery at D110, E116, and R117 partially rescues CFTR to open burst stability. (A–C) Representative single-channel currents of D110R- and D110E- (A), E116R- and E116D- (B), and R117A- and R117K-CFTR (C) recorded under the same conditions as Fig. 2 A. Their all-points amplitude histograms are shown on the right. (D) Mean single-channel amplitude of WT-, D110R-, D110E-, E116R-, E116D-, R117A-, and R117K-CFTR. *, P < 0.05 compared with WT-CFTR. (E) Mean burst duration of WT-, D110R-, D110E-, E116R-, E116D-, R117A-, and R117K-CFTR. #, P < 0.001 indicates differences between D110R- and D110E-CFTR or E116R- and E116D-CFTR; *, P < 0.05 indicates differences between R117A- and R117K-CFTR. n = 4-6 for all mutants. Mean \pm SEM is shown.

that it occupied mainly the f open state with rare s1 and s2 events and exhibited a significantly smaller singlechannel amplitude than WT-CFTR (-0.40 ± 0.02 pA, n = 4, P < 0.01 vs. WT). Mean burst duration of R104E-CFTR was 325 ± 54.08 ms, significantly shorter than WT but significantly longer than E116R-CFTR (Fig. 9 A, right). Single-channel behavior of the double mutant R104E/ E116R-CFTR was similar to R104E-CFTR, with a long, stable f open state and a mean burst duration significantly longer than that of E116R-CFTR (Fig. 9 A, right). Although the charge swap mutant did not fully recover WT-CFTR behavior, its recovery compared with E116R-CFTR suggests that E116 may form a salt bridge with R104 when CFTR channels are in the open state. In contrast, single-channel properties of the R104E/D110R-CFTR double mutant were not significantly different from the D110R-CFTR single mutant (Fig. S5), suggesting no interaction between R104 and D110.

To further test the possible salt bridge between R104 and E116, we made use of MTS reagents that we used previously to confirm interactions between R352C and D993C (Cui et al., 2013). We reasoned that if a salt bridge between R104 and E116 is important for stabilizing the open state, the bifunctional linker MTS-2-MTS may lock the cysteine-substituted double mutant R104C/E116C-CFTR into the full open state by covalently binding to both engineered cysteines. Surprisingly, without addition of MTS-2-MTS, in the presence of ATP and PKA

alone, R104C/E116C-CFTR exhibited very long stable openings with brief closed states and s1 and s2 subconductance states (Fig. 9 B, control). Measurement of the fraction of burst duration contributed by s1, s2, and f states under these conditions indicated that the channel occupied the f state >98% of the open time (Fig. 9 B, right). The mean burst duration of the double mutant was 1874.47 ms, much longer than WT-CFTR (683 ms). Consistent with this, its opening rate was significantly lower than WT-CFTR $(0.78\pm0.08 \text{ vs. } 2.08\pm0.58 \text{ openings/s/}$ channel, P < 0.05, n = 4-5), which likely reflects the approximately threefold longer burst duration in the mutant (Wang et al., 2005). These data suggest that the two engineered cysteines form a spontaneous disulfide bond when the channel is in the open state. This phenomenon has been observed in the acid-sensing ion channel 1 (ASIC1), where cysteines engineered at positions 110 and 428 result in spontaneous formation of a disulfide bond that traps the channel into the desensitized conformation (Springauf et al., 2011).

If the long openings of R104C/E116C-CFTR were caused by the formation of a spontaneous disulfide bond, then the reducing agent DTT should break the disulfide bond and modify the channel behavior. To test this idea, we added 1 mM DTT to the pipette solution and recorded single-channel current with ATP and PKA in the intracellular solution (Fig. 9 B, left, middle trace). In the presence of DTT, burst durations were much shorter.

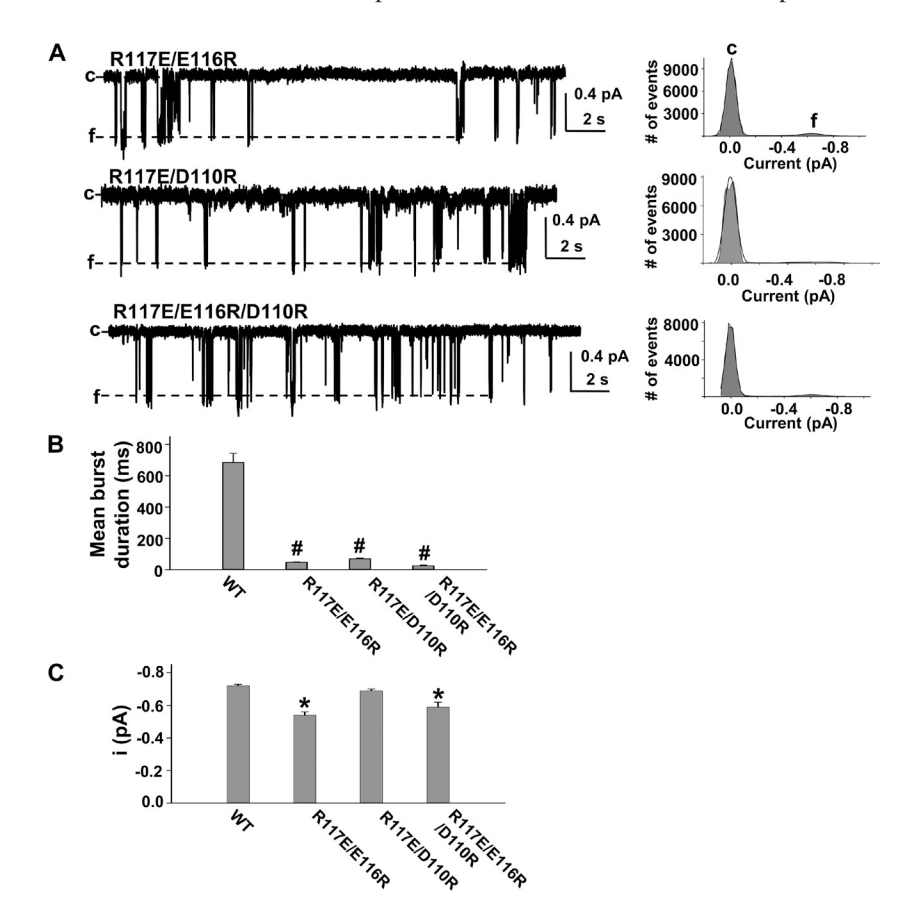


Figure 8. R117, E116, and D110 do not interact with each other locally to affect open pore architecture of CFTR. (A) Representative single-channel currents of R117E/E116R-, R117E/D110R-, and R117E/E116R/D110R-CFTR and corresponding all-points amplitude histograms recorded under the same conditions as Fig. 2 A. (B) Mean burst duration of WT-CFTR and the three compound mutants. #, P < 0.001 compared with WT-CFTR. n = 4–6 for all mutants. (C) Mean single-channel amplitudes of WT-, R117E/E116R-, R117E/D110R-, and R117E/E116R/D110R-CFTR. *, P < 0.05 compared with WT-CFTR. Mean \pm SEM is shown.

In addition, analysis of the fraction of burst duration represented by s1, s2, and f states after DTT exposure showed that both s1 and s2 were occupied much more often, whereas fractional occupancy of the f state was dramatically decreased (Fig. 9 B, right). These data strongly support the notion that the engineered cysteines at positions 104 and 116 form a spontaneous disulfide bond when the channel is in the open state.

To test this idea further, we preincubated oocytes expressing R104C/E116C-CFTR with 5 mM MTSET⁺ for

10 min before recording. MTSET⁺ binding to either cysteine at 104 or 116 would disrupt formation of the disulfide bond between them, resulting in single-channel behavior similar to that seen in the presence of DTT (Zhang et al., 2005a). A representative sample trace is shown in Fig. 9 B (left, bottom trace). Burst analysis indicated that channels primarily occupied the s1 and s2 states, whereas f state occupancy was dramatically decreased compared with control conditions; the latter finding may result from steric hindrance induced by labeling with MTSET⁺.

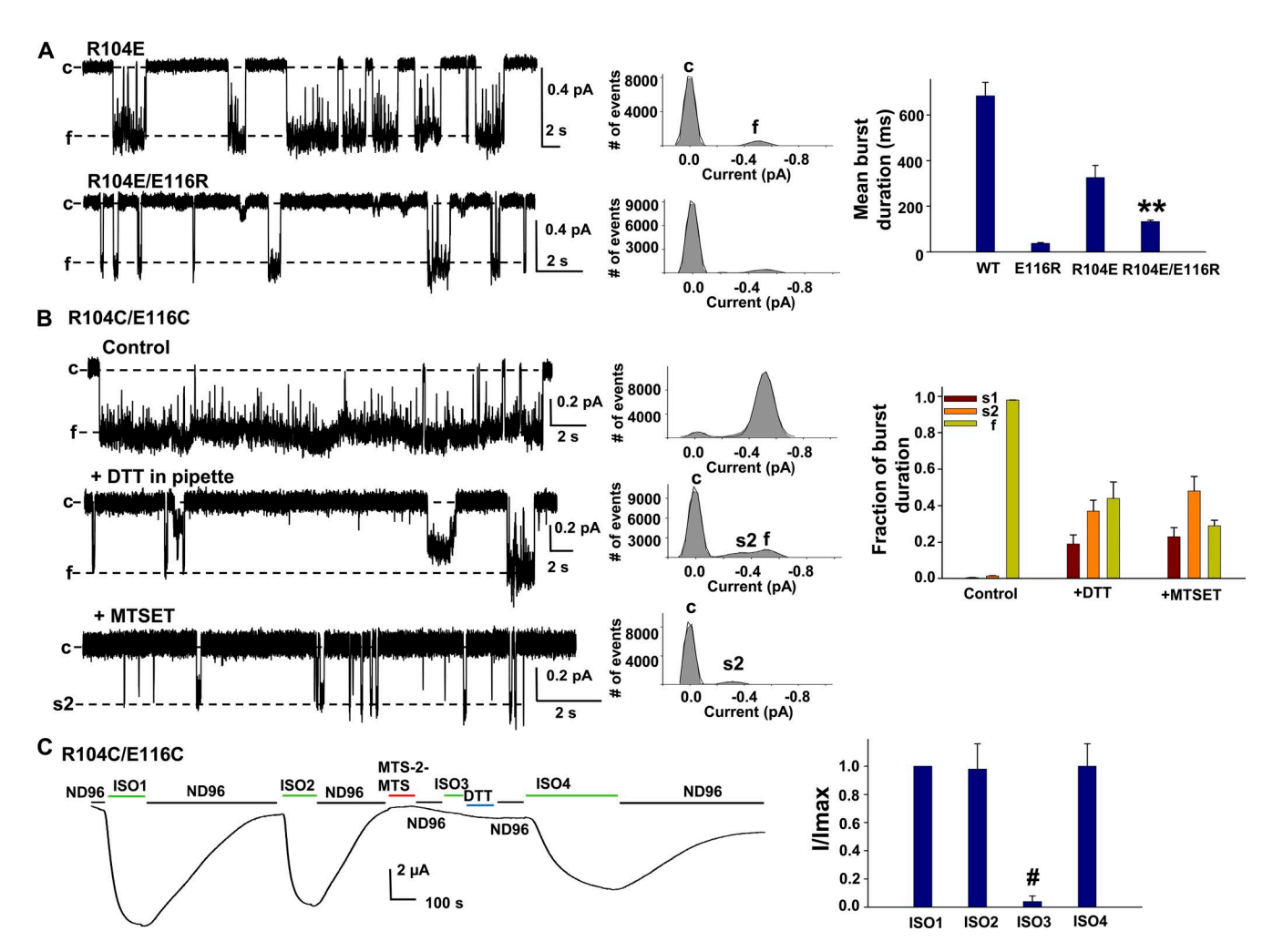


Figure 9. E116 forms a salt bridge with R104 in both the closed and open states. (A) Representative single-channel current traces of R104E- and R104E/E116R-CFTR recorded with the same experimental conditions as Fig. 2 (left), their all-points amplitude histograms (middle), and mean burst durations (right). ***, P < 0.01 indicates a significant difference between E116R- and R104E/E116R-CFTR. (B) Two cysteines engineered at positions 104 and 116 (R104C/E116C) form a spontaneous disulfide bond when CFTR is in the open state. Representative single-channel trace of R104C/E116C-CFTR recorded with the same conditions as A. Control, 150 mM Cl⁻ extracellular solution alone (left, top trace). DTT, dithiothreitol reducing agent. +DTT in pipette: R104C/E116C-CFTR recorded with 1 mM DTT in the extracellular pipette solution (left, middle trace). In the bottom trace, oocytes expressing R104C/E116C-CFTR were incubated in solution containing 5 mM MTSET⁺ over 10 min before single-channel current recording (+MTSET; left, bottom trace). Their all-points amplitude histograms are shown in the middle panel. Mean fraction of open burst duration is plotted at right for R104C/E116C-CFTR under three different experimental conditions, for each of the open conductance states: s1, dark red; s2, orange; and f, light green. (C) Cross-linking R104C to E116C using MTS-2-MTS locks CFTR channels into the closed state. Representative trace (left) and summary data (right) for macroscopic currents measured from R104C/E116C-CFTR with addition of 1 mM MTS-2-MTS in the absence of ISO at $V_M = -60$ mV. ND96, control bath solution. Current levels in the summary data chart are given relative to control conditions before first exposure to ISO and normalized to maximal current in response to ISO1. #, P < 0.001 compared with ISO1 in P = 4 experiments. Mean P < 0.001 compared with ISO1 in P < 0.001 compared w

However, MTSET⁺ did not induce a change in singlechannel conductance of the f open state. The data thus far suggest that (a) R104 and E116 form a salt bridge when the channel is in the open state. The required proximity for a salt bridge is confirmed by our finding that the thiol groups of two engineered cysteines at these positions are in close enough proximity in the open state to form a spontaneous disulfide bond (\sim 2–3 Å); (b) R104C and/or E116C do not contribute directly to ion conduction and permeation through CFTR because both could be modified by MTSET without affecting channel conductance. In support of this, we found no detectable change in the macroscopic current of E116C-CFTR upon exposure to MTSET (Fig. 4), consistent with the notion that these ECL1 amino acids do not directly contribute to ion conduction and permeation in CFTR (Gao et al., 2013).

The R104C/E116C spontaneous open state disulfide bond exhibited the following characteristics: (a) R104C/ E116C-CFTR still required ATP and PKA for activation. (b) R104C/E116C-CFTR exhibited an intraburst closed state even in the absence of DTT that is long enough to represent true channel closures, suggesting that the spontaneous disulfide bond is not strong enough to lock the channel into the open state but rather the channel is still affected by NBD-mediated gating, although to a much lower degree than the WT. This is in contrast to the ability of MTS-2-MTS to lock R352C/D993C-CFTR into the open state or to lock R334C/E217C-CFTR into the closed state (Cui et al., 2013; Rahman et al., 2013). These results support the notion that R104 interacts with E116 in the open state; approaching close enough to form a spontaneous disulfide likely precludes crosslinking by MTS-2-MTS.

Homology modeling and simulation predict that R104 and E116 might remain very close to each other and form a salt bridge when the channel is in the closed state as well; we therefore asked whether the bifunctional crosslinker MTS-2-MTS would lock R104C/E116C-CFTR closed when applied in the closed state. Representative data are shown in Fig. 9 C. R104C/E116C-CFTR could be reversibly activated and reactivated by ISO (ISO1 and ISO2) without significant decrement. We then exposed the cell to 1 mM MTS-2-MTS for 2 min when the channel was in the closed state (in the absence of ISO) and then attempted to reactivate with a third ISO exposure. MTS-2-MTS locked the channels into the closed state such that they could only be activated by ISO again after DTT was used to break the disulfide bond (summary data are shown in Fig. 9 C, right). The data strongly suggest that R104 forms a salt bridge with E116 in the closed state and therefore that the distance between these two amino acids is in the order of 4.6 Å, similar to other salt bridges (Cui et al., 2008). The closed state MTS-2-MTS cross-link bond also showed a clear difference from the R104C/E116C open state spontaneous disulfide bond, in that the former is much stronger and the energy released from ATP binding at the NBDs is not enough to break it, whereas the open state spontaneous disulfide bond can be broken by ATP hydrolysis during NBD-mediated gating. Collectively, these results indicate that R104 and E116 interact in both the closed and open states, and gating transitions between the closed and open states require transient interruption of this interaction.

D110 interacts with K892 when CFTR is in the closed state D110 was predicted in our new model to form a salt bridge with K892 in ECL4 when the channels are in the closed state (Rahman et al., 2013). To test this prediction, we made the single mutation K892E and the double mutation D110R/K892E. K892E-CFTR open channels behaved similarly to WT-CFTR, including displaying a stable full open state with single-channel amplitude similar to WT (-0.77 ± 0.02 pA, n = 5; Fig. 10), outward rectification in the I-V relationship, and WT-like reversal potential (Fig. S4 C and Table 1). These data suggest that K892 does not directly affect Cl⁻ ion conduction. The double mutant D110R/K892E-CFTR behaved similarly to D110R-CFTR (Fig. 7 A), displaying flickery openings to the s1, s2, and f states with a very brief open burst duration (Fig. 10 A). F-state amplitude in this mutant was -0.81 ± 0.02 pA (n = 4). The failure of the chargeswapping double mutant to recover WT open-channel behavior suggests that K892 and D110 do not interact in the open state. However, D110 does appear to be important in stabilizing the open state by some other means.

In our closed state model (C0 state, NBDs fully dedimerized), we noted that D110 and K892 are located very close to each other, suggesting that they might interact (Rahman et al., 2013). We hypothesized that if D110 forms a salt bridge with K892 in the closed state, then engineered cysteines at these positions might form a spontaneous disulfide bond to lock the channel into a fully closed state. To test this, we made the double cysteine mutant D110C/K892C-CFTR. Its single-channel behavior was very similar to that of D110R-CFTR except with a longer mean burst duration, probably because the cysteine at position 110 carries a partial negative charge that stabilizes channel open pore architecture in the same manner as D110 does (Fig. 10 A). The data also suggested that at least some of the double mutant D110C/K892C-CFTR channels could be activated by ATP and PKA in the absence of DTT, which would not support the formation of a stable spontaneous disulfide bond. To resolve this, we backfilled 1 mM DTT in the pipette solution and recorded single-channel current of WT- and D110C/K892C-CFTR from inside-out patches in the presence of cytosolic ATP and PKA, whereas DTT diffused to the tip. Representative experiments and summary data are shown in Fig. 10 (B and C). WT-CFTR exhibited similar single-channel behavior in the absence and presence of DTT. However, patches from oocytes expressing D110C/K892C-CFTR exhibited a very large increase in apparent channel number after exposure to extracellular DTT, consistent with channels being released from the spontaneous disulfide bond and therefore able to open. We analyzed window current each minute sequentially during phosphorylation by PKA and during diffusion of DTT to the tip, and plotted the time course (Fig. 10 B, right). WT-CFTR current activation was fit

with a single exponential function with $\tau=5.33$ min, which suggests that it takes \sim 7–8 min for WT-CFTR current to reach its plateau. D110C/K892C-CFTR patch current remained low in the first \sim 5 min, then slowly increased over the next 10–15 min as more channels were activated and the number of apparent channels in the patch increased (Fig. 10 C). The data were unable to be fit with an exponential, and the green line in Fig. 10 B (right) is a nonlinear regression fit. These results suggest that

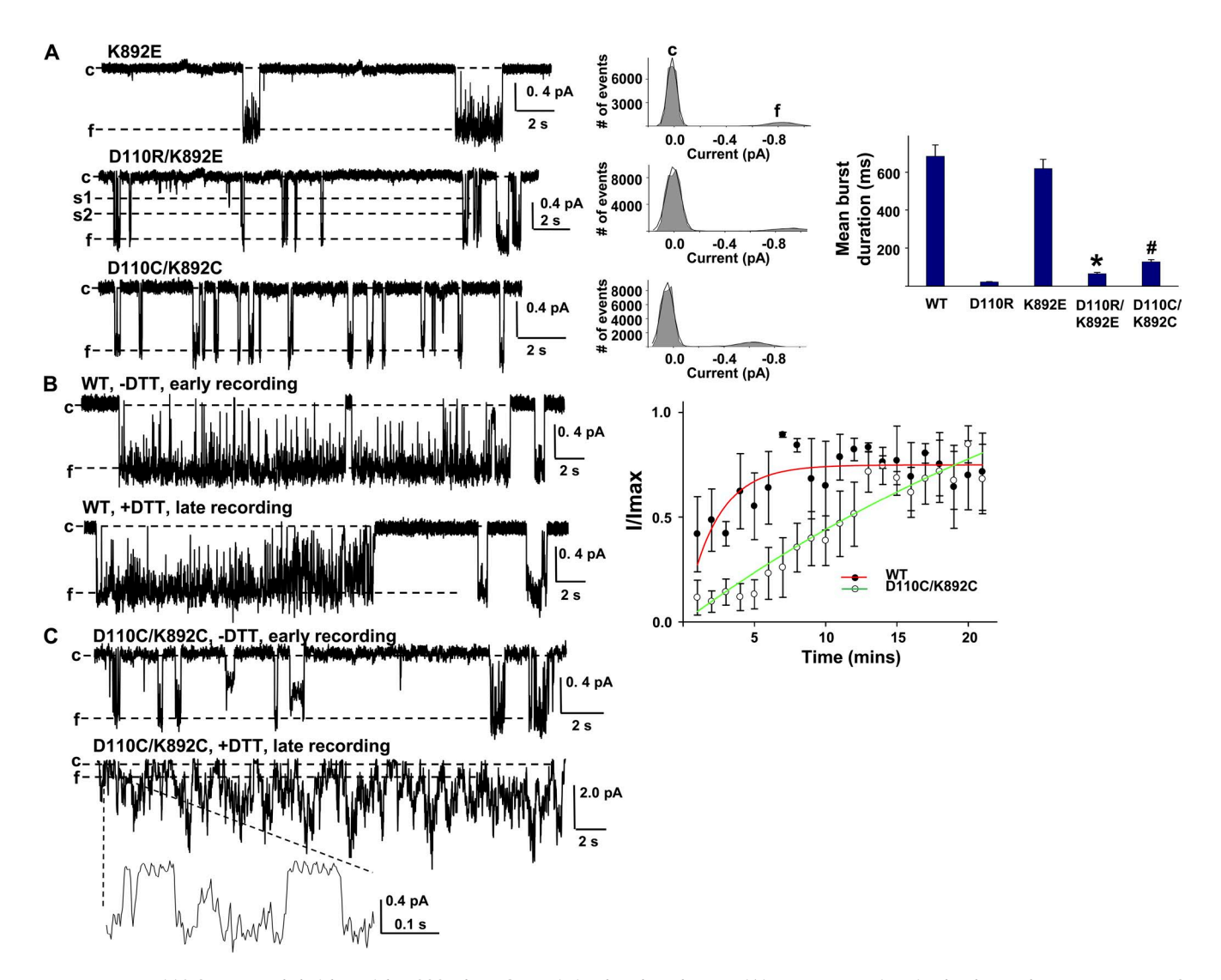


Figure 10. D110 forms a salt bridge with K892 when CFTR is in the closed state. (A) Representative single-channel current traces of K892E-, D110R/K892E-, and D110C/K892C-CFTR recorded with the same experimental conditions as Fig. 2 (left), their all-points amplitude histograms (middle), and their mean burst durations (right). *, P < 0.05 indicates a significant difference between D110R-and D110R/K892E-CFTR; #, P < 0.001 for D110C/K892C-CFTR compared with D110R alone. (B) Exposure to 1 mM DTT backfilled into the pipette had no effect on WT-CFTR. Two traces recorded from the same inside-out patch from a WT-CFTR–expressing oocyte at $V_M = -100$ mV, with MgATP and PKA in the intracellular solution. -DTT, DTT in the pipette solution but early in the recording; +DTT, late in the recording after DTT perfused to the tip of pipette. Window current every 1 min was measured with Clampfit 10.2 and normalized to the maximum window current (I_{max}). I/ I_{max} is plotted with its real time scale shown in the right panel. The data for WT-CFTR were fit with a single-exponential function with $\tau = 5.33$ min (red line). (C) Exposure to 1 mM DTT, backfilled into the pipette, increased the number of active channels in D110C/K892C-CFTR. Two traces recorded from the same inside-out patch at $V_M = -100$ mV, with MgATP and PKA in the intracellular solution. The third trace is a small part of the second trace expanded for viewing. -DTT, pipette solution alone; +DTT, DTT perfused to the tip of pipette. Window current data were fit using nonlinear regression, and no time constant was determined (green line). Mean \pm SEM is shown.

unlike WT-CFTR, D110C/K892C-CFTR was modified by DTT when it perfused to the pipette tip over 5–10 min during channel phosphorylation; DTT probably broke the disulfide bond between D110C and K892C, allowing more channels to be activated by ATP and PKA. The single-channel current amplitude of D110C/K892C-CFTR remained unchanged in the absence and presence of DTT; individual single-channel openings in the presence of DTT could not be distinguished from those in channels that were able to open before DTT. The distance between D110 and K892 in the C1 state in our CFTR homology model simulation was predicted to be \sim 15 Å, far larger than the distance between two amino acids in a disulfide bond (Rahman et al., 2013). However, in the C0 state of our simulation, with NBDs fully dedimerized, D110 and K892 are within van der Waals distances. Collectively, the data suggest that D110C/ K892C-CFTR forms a spontaneous disulfide bond when the channel is in the closed state (C0), and this locks the channel closed.

We further tested the spontaneous disulfide bond in D110C/K892C-CFTR with the macropatch technique. We pulled inside-out macropatches from oocytes expressing WT- or D110C/K892C-CFTR and recorded the current in real time during exposure to 1 mM DTT backfilled into the pipette. Representative currents and summary data are shown in Fig. 11 A. In WT-CFTR, channels were activated with ATP and PKA, reached plateau in \sim 5 min (Fig. 11 A, b), and exhibited a slight decrease over the next \sim 20 min as the result of rundown (Fig. 11 A, c; P < 0.01 comparing points b and c). For D110C/ K892C-CFTR ATP- and PKA-activated channels, but unlike WT-CFTR, D110C/K892C-CFTR currents slowly increased over the full duration of the experiment (\sim 20 min; Fig. 11 A, c). Both WT- and D110C/K892C-CFTR currents could be completely abolished with removal of ATP and PKA from the intracellular solution (Fig. 11 A, d). Representative I-V plots at the outset of recording and at 5 and 20 min in WT- and D110C/K892C-CFTR are shown in the middle panel of Fig. 11 A. Unlike WT-CFTR, D110C/K892C-CFTR exhibited strong inward rectification in symmetrical 150 mM Cl⁻ solution. The current increase in D110C/K892C-CFTR after ATP and PKA activation was likely caused by DTT-mediated breaking of disulfide bonds between D110C and K892C, allowing more channels to be activated and resulting in a higher current amplitude. Meanwhile, the data also suggest that not all D110C/K892C-CFTR channels formed disulfide bonds in the resting state and that some channels could be activated by ATP and PKA in the absence of DTT. As a control, in the absence of DTT, D110C/K892C-CFTR macroscopic current reached plateau in ~5 min (like WT-CFTR) and was maintained or slightly decreased in the next \sim 20 min (Fig. S7 A).

Because the above data were all from inside-out patches, where channels were exposed to ATP-free conditions

for several minutes, the question remained as to whether D110C/K892C-CFTR channels form a spontaneous disulfide bond in intact cells where CFTR is in the constant presence of ATP. We addressed this question in whole oocytes with the TEVC technique (Fig. 11, B and C). In WT-CFTR, addition of 1 mM DTT to ISO caused no increase in macroscopic current compared with ISO alone (Fig. 11 B). In contrast, in D110C/K892C-CFTR, activation by ISO plus DTT (ISO2 + DTT) led to significantly higher current than ISO alone (ISO1). These data suggest that in whole oocytes, a fraction of D110C/ K892C channels formed disulfide bonds under resting conditions and were locked into the closed state (C0). This group of channels could not be activated by ISO alone in the absence of DTT, but the disulfide bonds were broken by 1 mM DTT and the previously locked channels could then be activated. We then asked whether DTT could further activate D110C/K892C-CFTR current if we used DTT before ISO. We used 1 mM DTT alone for 3 min followed by ISO alone (ISO1), which fully activated D110C/K892C-CFTR channels to plateau. We then allowed channels to deactivate by washout in ND96 solution and applied ISO plus 1 mM DTT (ISO2 + DTT) to activate the channels again. The second macroscopic current amplitude was significantly smaller than ISO1 (Fig. 11 C). These data suggest that with prior DTT treatment, disulfide bonds formed during the closed state in D110C/K892C-CFTR were broken by DTT and ISO1 was able to activate all channels to reach maximum current. In the second activation, DTT plus ISO did not further increase the current amplitude (Fig. 11 C). In fact, the current amplitude of ISO2 + DTT was significantly decreased compared with ISO1, possibly as the result of rundown during this long experiment (Fig. 11 C, right). WT-CFTR macroscopic current amplitude also was slightly decreased in the second ISO + DTT activation compared with ISO1, regardless of whether oocytes were previously treated with DTT (Fig. S7 B). In the absence of 1 mM DTT, D110C/K892C-CFTR channels were activated by ISO1 and ISO2 to a similar level (Fig. S7 C), suggesting that ISO alone was not able to break the spontaneous disulfide bond between K892C and D110C in channels that had formed this bond.

In summary, the above data, combined with molecular modeling, suggest three important findings: (1) D110 forms a salt bridge with K892 in the closed state; (2) D110C/K892C-CFTR forms a spontaneous disulfide bond when the channel is in the closed state and the energy of CFTR channel gating is not strong enough to break it in the absence of the reducing agent DTT; (3) CFTR may transition to a state where the NBDs are fully dedimerized (C0 closed state), as our simulations suggest that C0 is the only state where these residues approach each other closely enough for a spontaneous disulfide to form.

We also tested the possibility that E116 could form an open state salt bridge with K892. E116R/K892E-CFTR exhibited an I-V relationship similar to that of WT-CFTR. The burst behavior of E116R/K892E-CFTR was similar to that of E116R-CFTR, suggesting that E116 does not form a salt bridge with K892 when the CFTR channel is in the open state (Fig. S5).

R117 interacts with E1126 when the CFTR channel is in the open state

Again informed by our model, we next tested the possibility of an open state salt bridge between R117 and E1126. Sample current traces for both E1126R- and R117E/E1126R-CFTR are shown in Fig. 12 A. As mentioned previously, we did not detect current from R117E-CFTR

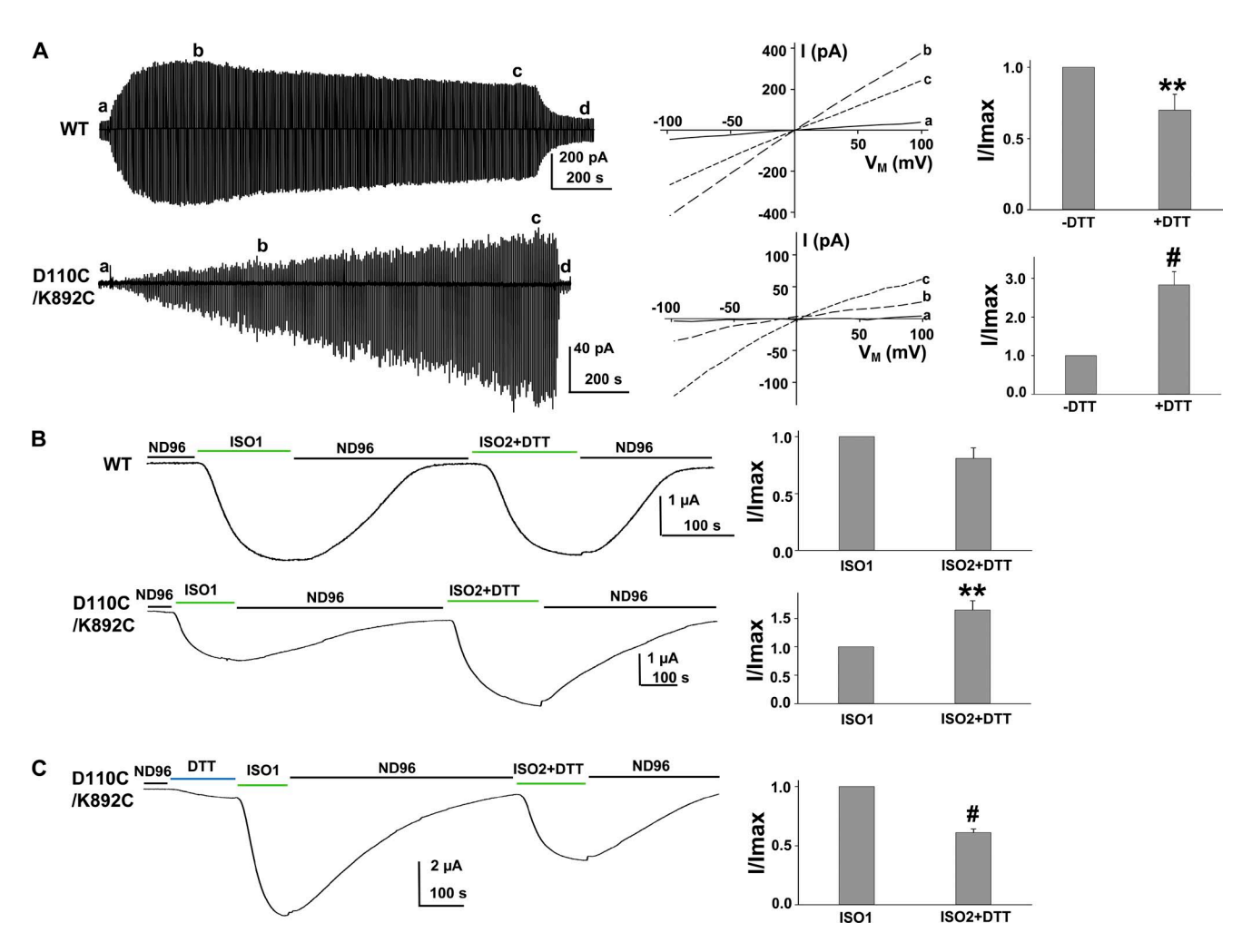


Figure 11. D110C forms a spontaneous disulfide bond with K892C when channels are in the closed state. (A) Representative macropatch currents of WT- and D110C/K892C-CFTR were recorded in inside-out mode with symmetrical 150 mM Cl⁻ solution. Pipette was backfilled with 1 mM DTT solution. A voltage protocol that held at 0 mV then stepped to 100 mV for 30 ms followed by a ramp to -100 mV over 300-ms duration was applied every 5 s. a, control, before ATP + PKA; b, peak current (I_{max}), with cytoplasmic ATP + PKA; c, current after DTT perfused fully to the tip of pipette, with cytoplasmic ATP + PKA; d, current with DTT perfused to the tip of pipette, wash out of cytoplasmic ATP + PKA. I-V plots of currents at times a-c for both WT- and D110C/K892C-CFTR are shown in the middle panel. Summary data are shown in the right panel. I_{max}, maximum current activated by ATP and PKA, likely before DTT perfused fully to the tip of pipette; I, current activated by ATP and PKA with DTT perfused to the tip of pipette. **, P < 0.01 indicates a significant difference in the pre- and post-DTT conditions; #, P < 0.001 indicates a significant difference in the pre- and post-DTT conditions. (B) 1 mM DTT further activated D110C/K892C-CFTR current but not WT-CFTR current in TEVC recording condition. Representative traces (left) and summary data (right) for macroscopic currents measured from WT- and D110C/K892C-CFTR with addition of 1 mM DTT in the presence of ISO. ND96, control bath solution. V_M = -60 mV. ISO1, 10 µM ISO alone; ISO2 + DTT, $1\ mM\ DTT\ in\ 10\ \mu M\ ISO\ solution.\ Current\ levels\ in\ the\ summary\ data\ are\ given\ relative\ to\ control\ conditions\ before\ first\ exposure\ to$ ISO and normalized to maximal current in response to ISO1 (I_{max}). **, P < 0.01 compared with ISO1 in n = 4 for WT-CFTR and n = 5for D110C/K892C-CFTR experiments. (C) ISO plus DTT failed to further activate D110C/K892C-CFTR current in oocytes pretreated with DTT in TEVC recording condition. Representative trace (left) and summary data (right) for macroscopic currents measured from D110C/K892C-CFTR with prior addition of 1 mM DTT for 3 min in ND96 solution. Current levels in the summary data are given relative to control conditions before first exposure to ISO and normalized to maximal current in response to ISO1 (I_{max}). #, P < 0.001 compared with ISO1 in n = 4 experiments. Mean \pm SEM is shown.

in oocytes. E1126R-CFTR mainly opened to the full open state but with frequent brief transitions to the s1 and s2 states. R117E/E1126R-CFTR opened to a full open state much more often compared with R117A-CFTR (Fig. 2). Mean burst duration for both E1126R- and R117E/E1126R-CFTR are summarized in Fig. 12 B. The mean burst duration of R117E/E1126R-CFTR was significantly longer than that of R117A- and R117C-CFTR. However, as noted previously for R104E/E116R-CFTR, the charge swap mutant did not completely recover the behavior of

WT-CFTR. The single-channel amplitudes of R117C- and R117C/E1126C-CFTR were slightly, but significantly, smaller than that of WT-CFTR (Fig. 12 C). We also compared the fractional burst duration represented by s1, s2, and f states for E1126R- and R117E/E1126R-CFTR and found that E1126R exhibited a significantly higher fraction of both s1 and s2 states than WT, whereas the distribution for double mutant R117E/E1126R-CFTR was similar to WT-CFTR, exhibiting mainly the f state (a nearly complete rescue; Fig. 12 D). These data suggest that

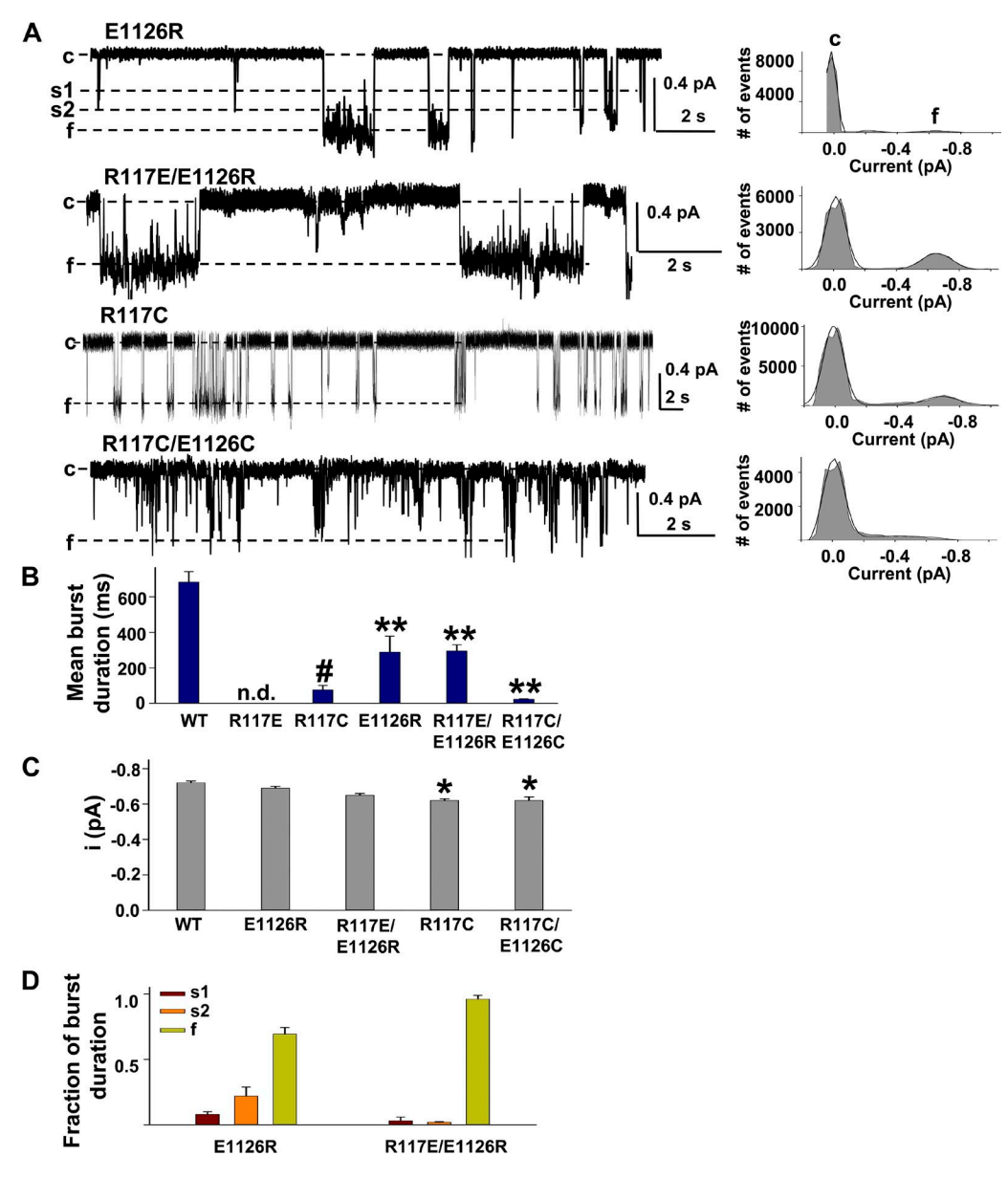


Figure 12. R117 forms a salt bridge with E1126 in the open state. (A) Representative single-channel current traces of E1126R-, R117E/E1126R-, R117C-, and R117C/E1126C-CFTR recorded under the same experimental conditions as Fig. 2 and their all-points amplitude histograms (right). (B) Mean burst durations of WT-CFTR and the above mutants. #, P < 0.01 indicates a significant difference between WT- and R117C-CFTR; **, P < 0.01 indicates a significant difference between WT- and E1126R-CFTR, between R117C and R117E/E1126R-CFTR, and between R117C and R117C/E1126C. n.d., no current detected for R117E-CFTR in *Xenopus* oocytes. n = 4-6 each. (C) Single-channel amplitudes of WT-CFTR and mutants. *, P < 0.05 compared with WT-CFTR. (D) Mean fraction of open burst duration is plotted for each open conductance state of E1126R- and R117E/E1126R-CFTR. Mean ± SEM is shown.

R117 may interact with E1126 to form a weak salt bridge that contributes to maintaining the open pore architecture in CFTR.

To further test the existence of a possible open state salt bridge between R117 and E1126, we again asked whether cysteines engineered at positions 117 and 1126 might form a disulfide bond as in R104C/E116C- or D110C/K892C-CFTR. R117C/E1126C-CFTR exhibited very brief openings to multiple open states, including s1, s2, and f, with significantly shorter mean burst duration compared with R117C-CFTR (P < 0.01), likely caused by mutual repulsion by the partial negative charges at the two cysteines, leading to unstable open states (Fig. 12, A and B). This suggests that the two cysteines at positions 117 and E1126 are not close enough to each other in the open state to form a spontaneous disulfide bond or that the disulfide bond formed is too weak to stabilize channel gating. In summary, (a) R117 forms a weak salt bridge with E1126 when the channel is in the open state; (b) the two cysteines engineered in positions 117 and 1126 are not close enough in the open state to form a spontaneous disulfide bond.

DISCUSSION

The major findings in this study can be summarized as follows: (a) the charged amino acids in ECL1 tested in this study (D110, D112, K114, E115, E116, and R117) are not directly involved in Cl⁻ permeation and conduction in CFTR; (b) D110, E116, and R117 strongly contribute to maintaining the outer pore architecture of CFTR by interacting with their salt bridge partners; (c) a cysteine residue introduced into TM1 at position 104 can form a spontaneous disulfide bond with a cysteine introduced into ECL1 at position 116 when the CFTR channel is in the open state. This bond breaks and forms again during the gating cycle of the NBDs such that R104 and E116 interact when the channel is in both the closed and open states; (d) D110 interacts with K892 of ECL4 when the CFTR channel is in the closed state (C0). Cysteines engineered at positions 110 and 892 form a spontaneous disulfide bond and keep the channel locked into the closed state until exposure to the reducing reagent DTT; (e) the charge at R117 interacts weakly with the charge at E1126 of ECL6 when the CFTR channel is in the open state, but cysteines introduced at these two sites do not form a spontaneous disulfide bond.

Movement of ECL1 during the gating cycle is restricted

ECL1 and ECL4 are the two longest loops among the six ECLs in CFTR, and their structures and function remain largely unexplored (Hämmerle et al., 2001; Chang et al., 2008). Based on the available homology models of CFTR, it is predicted that the outer pore domains are closely bundled together when the channel is in the closed state and disperse as the channel opens. We found that E116 of ECL1 forms a salt bridge with R104 of TM1 in both the closed and open states, and the two amino acids are very close to each other when the channel is in the open state because R104C only forms a spontaneous disulfide bond with E116C in this state. As shown here, mean burst durations of charge-retaining mutants D110E-, E116D-, and R117K-CFTR are significantly longer than their related charge-reversing or charge-destroying mutants D110R-, E116R-, and R117A-CFTR but distinctly shorter than that of WT-CFTR (Fig. 7). These data suggest that the structure of ECL1 must be tuned delicately to maintain function. Unlike the R352/D993 salt bridge, none of the charge-retaining mutations identified in ECL1 are able to completely rescue the mutant channel behavior to that of WT-CFTR. This is likely the result of a requirement for very specific bond angles within a network of charged residues that control the architecture of ECL1. Furthermore, because the R104-E116 salt bridge connects ECL1 to the extracellular end of TM1, we conclude that ECL1 moves a very limited distance or travels simultaneously with TM1 during CFTR's gating cycle.

Meanwhile, D110 appears to form a salt bridge with K892 of ECL4 and the D110C/K892C spontaneous disulfide bond can only be formed when the channel is in the C0 state (0-ns snapshot in our molecular dynamics simulation; Rahman et al., 2013). D110 and K892 widely

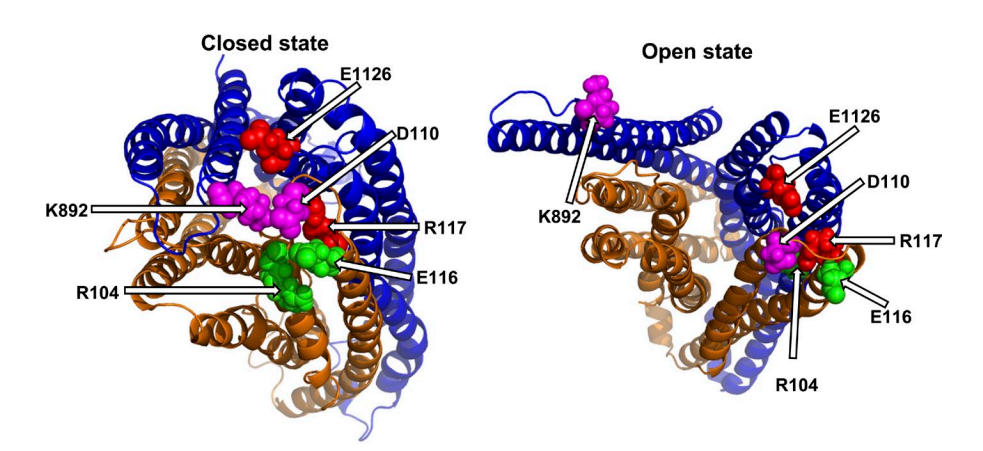


Figure 13. CFTR homology model with three pairs of interacting residues labeled in both closed and open states. Top view of the homology model (McCarty laboratory model; Rahman et al., 2013) with salt bridge residues shown as spheres: R117-E1126, red; E116-R104, green; and D110-K892E, magenta. (left) Closed state (equivalent to the state where the NBDs are fully dedimerized). (right) Open state. TM1-6 is indicated in brown shades, and TM7-12 is indicated in blue shades.

separate at 2.5 ns in the simulation. Because ECL1 moves only slightly during the closed to open gating transition, we surmise that ECL4 travels quite a distance away from ECL1, in a direction roughly perpendicular to the pore axis, when the CFTR channel opens (Fig. 13; Rahman et al., 2013). The other four ECLs in CFTR are very short and only contain a few amino acids each; therefore, they must move with or stay very close to their connected TM domains.

CFTR channels may visit a closed state with the NBDs fully dedimerized

The mechanism of ATP-dependent regulation of the CFTR gating cycle to control transitions between closed (C) and open (O) states has been researched extensively (Fuller et al., 2005; Hwang and Kirk, 2013). CFTR requires PKA to phosphorylate the R domain, followed by dimerization of the two NBDs (NBD1 and NBD2) in a head to tail dimer associated with occupancy of both composite ATP-binding sites 1 and 2 by ATP to open the CFTR pore. The CFTR gating cycle has been proposed to encompass the following scheme (Fig. S8): C0 (NBDs fully dedimerized and nucleotide free) \rightarrow C1 (ATP bound to site 1, NBDs partially dimerized) \rightarrow C2 (ATP bound to sites 1 and 2, NBDs fully dimerized) \rightarrow O1 (ATP bound at both sites, pore domain opened) \rightarrow O2 (ATP hydrolyzed at site 2, but not yet released) \rightarrow C3 (ATP bound at site 1, ADP bound at site 2, and channel closed but NBDs still dimerized) \rightarrow C4 (ATP bound at site 1, ADP bound at site 2, NBDs partially dimerized) → back to C1 (Csanády et al., 2010; Hwang and Kirk, 2013). The above C1, C2, C3, C4, O1, and O2 states have been extensively studied in the last \sim 20 years, and strong experimental data have accumulated in confirmation. However, with respect to the C0 state, to our knowledge there are no experimental data to date to support the notion that CFTR spends significant time in the fully NBD dedimerized closed state. Meanwhile, ABC transporter family members such as P-glycoprotein clearly display a fully NBD dedimerized state, which may approximate the C0 state in CFTR (Aller et al., 2009; Hunt et al., 2013; Rahman et al., 2013).

Through the majority of the 10 ns of molecular dynamics simulation of our CFTR homology model, D110 remains relatively stationary and forms a salt bridge with K892 only in the C0 closed state. K892 moves away from D110 immediately as the simulation progresses from C0 toward the open channel state, and at 2.5 ns is far away from D110 and unable to maintain the salt bridge (Fig. S8; Rahman et al., 2013). In the present work, we demonstrated that D110C/K892C-CFTR forms a spontaneous disulfide bond and appeared to lock the channel into the C0 state. The C0 state channel was not activated by PKA and ATP until DTT was used to break the disulfide bond, allowing the channel to open and close after normal NBD gating (Figs. 10, 11, and 13). In WT-CFTR, the existence of the C0 state has not been confirmed in

experiments thus far, likely because it is difficult to study closed channels because of the absence of electrical signature.

The data presented here suggesting the possible existence of the C0 state in the CFTR gating cycle clearly move CFTR (the only ion channel built on an ABC transporter platform) closer to the other members of the ABC family. Consequently, the existence of the C0 state may also suggest that CFTR might actually be a transporter that evolved the ability to switch to channel activity (Jordan et al., 2008; Cui et al., 2012; Sebastian et al., 2013). Questions remaining include: (a) what is the distance between the two NBDs in the dedimerized state in CFTR? The two NBDs in P-glycoprotein are separated by ~ 30 Å to fulfill a transporter function, whereas because CFTR is a channel, the distance between NBDs might be shorter as it would not have to open widely to accommodate substrate binding (Aller et al., 2009). (b) How long might it take in physiological conditions for CFTR to switch from C0 to C1 and vice versa? (c) Do the NBDs approach each other by traveling the same distance or is movement dominated by one of them? Further studies are underway to resolve these questions.

Two spontaneous disulfide bonds formed in CFTR mutants with different characteristics

Disulfide bonds play several roles including stabilizing protein structure, mediating catalytic thiol-disulfide exchange reactions, and affecting protein function allosterically by switching between bonded and unbonded states (Schmidt et al., 2006). The stability of disulfide bonds in small molecules and proteins varies across an enormous span of free energies ranging from 2.1 to 84.5 kJ/mol, depending on dihedral angle (Schmidt et al., 2006; DeCaen et al., 2008). Disulfide bonds show a distinct preference for a dihedral angle approaching 90° (Schmidt et al., 2006). The distance between two α -carbon atoms of the cysteine residues is often between 4.3 and 5.65 Å, whereas the sulfhydryls must approach to \sim 2 Å at the time of formation of a disulfide bond (Gilbert, 1995; Schmidt et al., 2006; DeCaen et al., 2008).

ATP hydrolysis is a highly exergonic process. When the terminal phosphate bond is broken in generation of ADP, 30.5 kJ/mol of energy (ΔG) is released, and when ATP hydrolysis occurs under cellular conditions the actual value of ΔG is closer to 50 kJ/mol (Hingorani et al., 1999; Sauna and Ambudkar, 2000). A disulfide bond formed between cysteines in the S2 segment and the S4 segment of the bacterial sodium channel NaChBac can be broken during voltage-activated gating (DeCaen et al., 2008). In contrast, G40C and E41C of KCNQ1 move very close to I145C of KCNE1 in the activated and resting states, respectively, and allow disulfide bond formation, which leads to formation of a KCNQ1 and KCNE1 channel complex that is stable until DTT is added to break the disulfide bonds (Xu et al., 2008).

In the current study, we identified two spontaneous disulfide bonds in CFTR formed after introduction of cysteines at positions 110 and 892 (a closed state disulfide bond in D110C/K892C-CFTR) or 104 and 116 (an open state disulfide bond in R104C/E116C-CFTR). These two disulfide bonds exhibited different stability during NBD-mediated gating. The D110C/K892C disulfide bond was maintained regardless of CFTR gating energy until the reducing agent DTT was added to break it. In contrast, the R104C/E116C disulfide bond was occasionally broken during normal NBD-mediated gating in the presence of ATP, although the closed state was rather brief. These data suggest that D110C/K892C-CFTR forms a very strong disulfide bond with dissociation energy that must be greater than that of ATP-dependent NBD dimer formation. In contrast, R104C/E116C forms a relatively weak disulfide bond, most likely because of its dihedral angle being dramatically off from 90°, and thus the dissociation energy is likely below that of ATP hydrolysis and subsequent NBD dedimerization.

ECLs differently contribute to CFTR channel function

In this study, we have investigated the functions of multiple amino acids of the ECLs in CFTR, including D110, D112, K114, E115, E116, and R117 of ECL1; D891, K892, and R899 of ECL4; and E1124 and E1126 of ECL6. Our experimental results lead us to the following conclusions about the structure and function of the ECLs in CFTR: (a) most charged amino acids in the ECLs are not directly involved in Cl⁻ conduction and permeation; (b) some important charged amino acids contribute to maintaining the outer pore architecture in CFTR, such as D110, E116, and R117; therefore, their disease-associated mutations may damage CFTR's outer pore architecture and as result cause reduced Cl⁻ flow; (c) it is absolutely necessary for ECL1 to maintain a finely tuned structure through the CFTR gating cycle; (d) according to our molecular dynamics simulation of CFTR gating, ECL4 moves the greatest distance away from the pore axis during the CFTR closed to open gating transition compared with other ECLs; disruption of the D110-K892 interaction allows ECL4 to move far away from ECL1 with CFTR channel opening, but the other five ECLs move with their connected TMs within a very limited distance (Rahman et al., 2013).

Potential CFTR extracellular blockers and openers for treating CFTR-related diseases

Ion channel blockers and activators (or openers) that work from the intracellular side have been largely studied and broadly used in the clinic, such as the L-type calcium channel blocker nifedipine, the KCNQ2/3 activators retigabine and flupirtine, the voltage-gated Na⁺ channel blocker lidocaine, and the CFTR channel potentiator VX-770 (Van Goor et al., 2009; Yu et al., 2012; Bagal et al., 2013). In contrast, small-molecule drugs that affect

ion channel function from the extracellular side are not well known. In fact, GlyH-101 is the first extracellular blocker of CFTR (Muanprasat et al., 2004), and benzo-furoindole is a large-conductance Ca²⁺-activated K⁺ channel extracellular opener that acts from the extracellular side of the membrane (Ha et al., 2006).

Drugs that target intracellular binding sites may have multiple effects resulting from the hydrophobicity required to permeate the plasma membrane. In contrast, drugs that target extracellular binding sites typically exhibit much simpler effects without otherwise affecting cellular physiology; this notion was supported by the study of GlyH-101 (Sonawane et al., 2006; Thiagarajah and Verkman, 2013). Identification of CFTR openers and blockers that function from the extracellular side may benefit patients suffering from CFTR-related diseases, including those with secretory diarrhea and CF. For example, if chemicals could lock the CFTR channel into the C0 state and preclude its activation in response to cholera toxin, the fluid loss in cholera patients would be dramatically reduced. Consequently, understanding the ECLs and the outer pore architecture of CFTR may be key in the development of CFTR-related pharmaceuticals. We will combine the CFTR homology model and molecular docking with experimental techniques to develop new therapeutics as our future direction.

This research was supported by research grant R01-DK056481 from the National Institutes of Health to N.A. McCarty.

The authors declare no competing financial interests.

Author contributions: G. Cui designed and carried out the electrophysiological measurements, analyzed data, prepared the figures, and wrote the manuscript. D.T. Infield was involved in designing experiments and contributed to manuscript preparation. C. Kuang and C.Z. Prince made all of the DNA constructs. K.S. Rahman made the CFTR homology model and predicted the possible amino acids pairs for the paper. C. Kuang performed surgery and prepared *Xenopus* oocytes. N.A. McCarty planned the project, designed experiments, and contributed to the manuscript preparation.

Merritt C. Maduke served as editor.

Submitted: 17 October 2013 Accepted: 19 June 2014

REFERENCES

Alexander, C., A. Ivetac, X. Liu, Y. Norimatsu, J.R. Serrano, A. Landstrom, M. Sansom, and D.C. Dawson. 2009. Cystic fibrosis transmembrane conductance regulator: using differential reactivity toward channel-permeant and channel-impermeant thiol-reactive probes to test a molecular model for the pore. *Biochemistry*. 48:10078–10088. http://dx.doi.org/10.1021/bi901314c

Aller, S.G., J. Yu, A. Ward, Y. Weng, S. Chittaboina, R. Zhuo, P.M. Harrell, Y.T. Trinh, Q. Zhang, I.L. Urbatsch, and G. Chang. 2009. Structure of P-glycoprotein reveals a molecular basis for poly-specific drug binding. *Science*. 323:1718–1722. http://dx.doi.org/10.1126/science.1168750

Bagal, S.K., A.D. Brown, P.J. Cox, K. Omoto, R.M. Owen, D.C. Pryde, B. Sidders, S.E. Skerratt, E.B. Stevens, R.I. Storer, and N.A. Swain.

- 2013. Ion channels as the rapeutic targets: a drug discovery perspective. J. Med. Chem. 56:593–624. http://dx.doi.org/10.1021/jm3011433
- Bai, Y., M. Li, and T.C. Hwang. 2010. Dual roles of the sixth transmembrane segment of the CFTR chloride channel in gating and permeation. *J. Gen. Physiol.* 136:293–309. http://dx.doi.org/10.1085/jgp.201010480
- Cestèle, S., V. Yarov-Yarovoy, Y. Qu, F. Sampieri, T. Scheuer, and W.A. Catterall. 2006. Structure and function of the voltage sensor of sodium channels probed by a beta-scorpion toxin. *J. Biol. Chem.* 281:21332–21344. http://dx.doi.org/10.1074/jbc.M603814200
- Chang, X.B., A. Mengos, Y.X. Hou, L. Cui, T.J. Jensen, A. Aleksandrov, J.R. Riordan, and M. Gentzsch. 2008. Role of N-linked oligosaccharides in the biosynthetic processing of the cystic fibrosis membrane conductance regulator. *J. Cell Sci.* 121:2814–2823. http:// dx.doi.org/10.1242/jcs.028951
- Cotten, J.F., and M.J. Welsh. 1999. Cystic fibrosis-associated mutations at arginine 347 alter the pore architecture of CFTR. Evidence for disruption of a salt bridge. *J. Biol. Chem.* 274:5429–5435. http://dx.doi.org/10.1074/jbc.274.9.5429
- Csanády, L., P. Vergani, and D.C. Gadsby. 2010. Strict coupling between CFTR's catalytic cycle and gating of its Cl⁻ ion pore revealed by distributions of open channel burst durations. *Proc. Natl. Acad. Sci. USA*. 107:1241–1246. http://dx.doi.org/10.1073/pnas.0911061107
- Cui, G., Z.R. Zhang, A.R. O'Brien, B. Song, and N.A. McCarty. 2008. Mutations at arginine 352 alter the pore architecture of CFTR. J. Membr. Biol. 222:91–106. http://dx.doi.org/10.1007/ s00232-008-9105-9
- Cui, G., B. Song, H.W. Turki, and N.A. McCarty. 2012. Differential contribution of TM6 and TM12 to the pore of CFTR identified by three sulfonylurea-based blockers. *Pflugers Arch.* 463:405–418. http://dx.doi.org/10.1007/s00424-011-1035-1
- Cui, G., C.S. Freeman, T. Knotts, C.Z. Prince, C. Kuang, and N.A. McCarty. 2013. Two salt bridges differentially contribute to the maintenance of cystic fibrosis transmembrane conductance regulator (CFTR) channel function. *J. Biol. Chem.* 288:20758–20767. http://dx.doi.org/10.1074/jbc.M113.476226
- DeCaen, P.G., V. Yarov-Yarovoy, Y. Zhao, T. Scheuer, and W.A. Catterall. 2008. Disulfide locking a sodium channel voltage sensor reveals ion pair formation during activation. *Proc. Natl. Acad. Sci. USA*. 105:15142–15147. http://dx.doi.org/10.1073/pnas.0806486105
- Delaunay, A., X. Gasull, M. Salinas, J. Noël, V. Friend, E. Lingueglia, and E. Deval. 2012. Human ASIC3 channel dynamically adapts its activity to sense the extracellular pH in both acidic and alkaline directions. *Proc. Natl. Acad. Sci. USA*. 109:13124–13129. http://dx.doi.org/10.1073/pnas.1120350109
- El Hiani, Y., and P. Linsdell. 2012. Tuning of CFTR chloride channel function by location of positive charges within the pore. *Biophys. J.* 103:1719–1726. http://dx.doi.org/10.1016/j.bpj.2012.09.020
- Fuller, M.D., Z.R. Zhang, G. Cui, and N.A. McCarty. 2005. The block of CFTR by scorpion venom is state-dependent. *Biophys. J.* 89:3960–3975. http://dx.doi.org/10.1529/biophysj.105.060731
- Fuller, M.D., C.H. Thompson, Z.R. Zhang, C.S. Freeman, E. Schay, G. Szakács, E. Bakos, B. Sarkadi, D. McMaster, R.J. French, et al. 2007. State-dependent inhibition of cystic fibrosis transmembrane conductance regulator chloride channels by a novel peptide toxin. J. Biol. Chem. 282:37545–37555. http://dx.doi.org/10.1074/jbc..M708079200
- Gabriel, S.E., K.N. Brigman, B.H. Koller, R.C. Boucher, and M.J. Stutts. 1994. Cystic fibrosis heterozygote resistance to cholera toxin in the cystic fibrosis mouse model. *Science*. 266:107–109. http://dx.doi.org/10.1126/science.7524148
- Gao, X., Y. Bai, and T.C. Hwang. 2013. Cysteine scanning of CFTR's first transmembrane segment reveals its plausible roles in gating and

- permeation. *Biophys. J.* 104:786–797. http://dx.doi.org/10.1016/j.bpj.2012.12.048
- Gilbert, H.F. 1995. Thiol/disulfide exchange equilibria and disulfide bond stability. *Methods Enzymol.* 251:8–28. http://dx.doi.org/10.1016/0076-6879(95)51107-5
- Glozman, R., T. Okiyoneda, C.M. Mulvihill, J.M. Rini, H. Barriere, and G.L. Lukacs. 2009. N-glycans are direct determinants of CFTR folding and stability in secretory and endocytic membrane traffic. J. Cell Biol. 184:847–862. http://dx.doi.org/10.1083/jcb.200808124
- Ha, T.S., H.H. Lim, G.E. Lee, Y.C. Kim, and C.S. Park. 2006. Electrophysiological characterization of benzofuroindole-induced potentiation of large-conductance Ca2+-activated K+ channels. *Mol. Pharmacol.* 69:1007–1014.
- Hämmerle, M.M., A.A. Aleksandrov, and J.R. Riordan. 2001. Diseaseassociated mutations in the extracytoplasmic loops of cystic fibrosis transmembrane conductance regulator do not impede biosynthetic processing but impair chloride channel stability. *J. Biol. Chem.* 276:14848–14854. http://dx.doi.org/10.1074/jbc.M011017200
- Hanrahan, J.W., J.A. Tabcharani, F. Becq, C.J. Mathews, O. Augustinas, T.J. Jensen, X.B. Chang, and J.R. Riordan. 1995. Function and dysfunction of the CFTR chloride channel. Soc. Gen. Physiol. Ser. 50:125–137.
- Hingorani, M.M., L.B. Bloom, M.F. Goodman, and M. O'Donnell. 1999. Division of labor—sequential ATP hydrolysis drives assembly of a DNA polymerase sliding clamp around DNA. *EMBO J.* 18:5131–5144. http://dx.doi.org/10.1093/emboj/18.18.5131
- Hunt, J.F., C. Wang, and R.C. Ford. 2013. Cystic fibrosis transmembrane conductance regulator (ABCC7) structure. Cold Spring Harb Perspect Med. 3:a009514. http://dx.doi.org/10.1101/cshperspect.a009514
- Hwang, T.C., and K.L. Kirk. 2013. The CFTR ion channel: gating, regulation, and anion permeation. *Cold Spring Harb Perspect Med.* 3:a009498. http://dx.doi.org/10.1101/cshperspect.a009498
- Jordan, I.K., K.C. Kota, G. Cui, C.H. Thompson, and N.A. McCarty. 2008. Evolutionary and functional divergence between the cystic fibrosis transmembrane conductance regulator and related ATP-binding cassette transporters. *Proc. Natl. Acad. Sci. USA*. 105:18865–18870. http://dx.doi.org/10.1073/pnas.0806306105
- Kristidis, P., D. Bozon, M. Corey, D. Markiewicz, J. Rommens, L.C. Tsui, and P. Durie. 1992. Genetic determination of exocrine pancreatic function in cystic fibrosis. Am. J. Hum. Genet. 50:1178–1184.
- Li, M.S., E.A. Cowley, and P. Linsdell. 2012. Pseudohalide anions reveal a novel extracellular site for potentiators to increase CFTR function. *Br. J. Pharmacol.* 167:1062–1075. http://dx.doi.org/ 10.1111/j.1476-5381.2012.02041.x
- Liu, X., S.S. Smith, F. Sun, and D.C. Dawson. 2001. CFTR: covalent modification of cysteine-substituted channels expressed in *Xenopus* oocytes shows that activation is due to the opening of channels resident in the plasma membrane. *J. Gen. Physiol.* 118:433–446. http://dx.doi.org/10.1085/jgp.118.4.433
- McCarty, N.A., and Z.R. Zhang. 2001. Identification of a region of strong discrimination in the pore of CFTR. Am. J. Physiol. Lung Cell. Mol. Physiol. 281:L852–L867.
- McCarty, N.A., S. McDonough, B.N. Cohen, J.R. Riordan, N. Davidson, and H.A. Lester. 1993. Voltage-dependent block of the cystic fibrosis transmembrane conductance regulator Cl⁻ channel by two closely related arylaminobenzoates. *J. Gen. Physiol.* 102:1–23. http://dx.doi.org/10.1085/jgp.102.1.1
- McDonough, S., N. Davidson, H.A. Lester, and N.A. McCarty. 1994. Novel pore-lining residues in CFTR that govern permeation and open-channel block. *Neuron.* 13:623–634. http://dx.doi.org/10.1016/0896-6273(94)90030-2
- McPhee, J.C., D.S. Ragsdale, T. Scheuer, and W.A. Catterall. 1998. A critical role for the S4-S5 intracellular loop in domain IV of the sodium channel α-subunit in fast inactivation. *J. Biol. Chem.* 273:1121–1129. http://dx.doi.org/10.1074/jbc.273.2.1121

- Mornon, J.P., P. Lehn, and I. Callebaut. 2008. Atomic model of human cystic fibrosis transmembrane conductance regulator: membrane-spanning domains and coupling interfaces. *Cell. Mol. Life Sci.* 65: 2594–2612. http://dx.doi.org/10.1007/s00018-008-8249-1
- Mornon, J.P., P. Lehn, and I. Callebaut. 2009. Molecular models of the open and closed states of the whole human CFTR protein. *Cell. Mol. Life Sci.* 66:3469–3486. http://dx.doi.org/10.1007/s00018-009-0133-0
- Muanprasat, C., N.D. Sonawane, D. Salinas, A. Taddei, L.J. Galietta, and A.S. Verkman. 2004. Discovery of glycine hydrazide pore-occluding CFTR inhibitors: mechanism, structure-activity analysis, and in vivo efficacy. J. Gen. Physiol. 124:125–137. http://dx.doi.org/10.1085/jgp.200409059
- Norimatsu, Y., A. Ivetac, C. Alexander, N. O'Donnell, L. Frye, M.S.P. Sansom, and D.C. Dawson. 2012. Locating a plausible binding site for an open-channel blocker, GlyH-101, in the pore of the cystic fibrosis transmembrane conductance regulator. *Mol. Pharmacol.* 82:1042–1055. http://dx.doi.org/10.1124/mol.112.080267
- Price, M.P., H. Ishihara, D.N. Sheppard, and M.J. Welsh. 1996. Function of *Xenopus* cystic fibrosis transmembrane conductance regulator (CFTR) Cl channels and use of human-*Xenopus* chimeras to investigate the pore properties of CFTR. *J. Biol. Chem.* 271:25184–25191. http://dx.doi.org/10.1074/jbc.271.41.25184
- Rahman, K.S., G. Cui, S.C. Harvey, and N.A. McCarty. 2013. Modeling the conformational changes underlying channel opening in CFTR. PLoS ONE. 8:e74574. http://dx.doi.org/10.1371/journal.pone.0074574
- Renauld, S., and A. Chraibi. 2009. Role of the C-terminal part of the extracellular domain of the α-ENaC in activation by sulfonylurea glibenclamide. *J. Membr. Biol.* 230:133–141. http://dx.doi.org/10.1007/s00232-009-9193-1
- Sauna, Z.E., and S.V. Ambudkar. 2000. Evidence for a requirement for ATP hydrolysis at two distinct steps during a single turnover of the catalytic cycle of human P-glycoprotein. *Proc. Natl. Acad. Sci. USA*. 97:2515–2520. http://dx.doi.org/10.1073/pnas.97.6.2515
- Schmidt, B., L. Ho, and P.J. Hogg. 2006. Allosteric disulfide bonds. *Biochemistry*. 45:7429–7433. http://dx.doi.org/10.1021/ bi0603064
- Sebastian, A., L. Rishishwar, J. Wang, K.F. Bernard, A.B. Conley, N.A. McCarty, and I.K. Jordan. 2013. Origin and evolution of the cystic fibrosis transmembrane regulator protein R domain. *Gene*. 523:137–146. http://dx.doi.org/10.1016/j.gene.2013.02.050
- Serohijos, A.W., T. Hegedus, A.A. Aleksandrov, L. He, L. Cui, N.V. Dokholyan, and J.R. Riordan. 2008. Phenylalanine-508 mediates a cytoplasmic-membrane domain contact in the CFTR 3D structure crucial to assembly and channel function. *Proc. Natl. Acad. Sci. USA*. 105:3256–3261. http://dx.doi.org/10.1073/pnas.0800254105
- Sheppard, D.N., D.P. Rich, L.S. Ostedgaard, R.J. Gregory, A.E. Smith, and M.J. Welsh. 1993. Mutations in CFTR associated with mild-disease-form Cl⁻ channels with altered pore properties. *Nature*. 362:160–164. http://dx.doi.org/10.1038/362160a0
- Shi, S., D.D. Ghosh, S. Okumura, M.D. Carattino, O.B. Kashlan, S. Sheng, and T.R. Kleyman. 2011. Base of the thumb domain modulates epithelial sodium channel gating. *J. Biol. Chem.* 286:14753–14761. http://dx.doi.org/10.1074/jbc.M110.191734
- Sonawane, N.D., J. Hu, C. Muanprasat, and A.S. Verkman. 2006. Luminally active, nonabsorbable CFTR inhibitors as potential therapy to reduce intestinal fluid loss in cholera. *FASEB J.* 20: 130–132.

- Springauf, A., P. Bresenitz, and S. Gründer. 2011. The interaction between two extracellular linker regions controls sustained opening of acid-sensing ion channel 1. *J. Biol. Chem.* 286:24374–24384. http://dx.doi.org/10.1074/jbc.M111.230797
- Stockand, J.D., A. Staruschenko, O. Pochynyuk, R.E. Booth, and D.U. Silverthorn. 2008. Insight toward epithelial Na⁺ channel mechanism revealed by the acid-sensing ion channel 1 structure. *IUBMB Life.* 60:620–628. http://dx.doi.org/10.1002/iub.89
- Sullivan, L.P., D.P. Wallace, and J.J. Grantham. 1998. Epithelial transport in polycystic kidney disease. *Physiol. Rev.* 78:1165–1191.
- Thiagarajah, J.R., and A.S. Verkman. 2013. Chloride channel-targeted therapy for secretory diarrheas. *Curr. Opin. Pharmacol.* 13:888–894. http://dx.doi.org/10.1016/j.coph.2013.08.005
- Van Goor, F., S. Hadida, P.D. Grootenhuis, B. Burton, D. Cao, T. Neuberger, A. Turnbull, A. Singh, J. Joubran, A. Hazlewood, et al. 2009. Rescue of CF airway epithelial cell function in vitro by a CFTR potentiator, VX-770. Proc. Natl. Acad. Sci. USA. 106:18825–18830. http://dx.doi.org/10.1073/pnas.0904709106
- Wang, J., V. Yarov-Yarovoy, R. Kahn, D. Gordon, M. Gurevitz, T. Scheuer, and W.A. Catterall. 2011. Mapping the receptor site for α-scorpion toxins on a Na⁺ channel voltage sensor. *Proc. Natl. Acad. Sci. USA*. 108:15426–15431. http://dx.doi.org/10.1073/pnas.1112320108
- Wang, W., G. Li, J.P. Clancy, and K.L. Kirk. 2005. Activating cystic fibrosis transmembrane conductance regulator channels with pore blockeranalogs. J. Biol. Chem. 280:23622–23630. http://dx.doi.org/10.1074/jbc.M503118200
- Weatherall, K.L., V. Seutin, J.F. Liégeois, and N.V. Marrion. 2011. Crucial role of a shared extracellular loop in apamin sensitivity and maintenance of pore shape of small-conductance calcium-activated potassium (SK) channels. *Proc. Natl. Acad. Sci. USA*. 108:18494–18499. http://dx.doi.org/10.1073/pnas.1110724108
- Xu, X., M. Jiang, K.L. Hsu, M. Zhang, and G.N. Tseng. 2008. KCNQ1 and KCNE1 in the IKs channel complex make state-dependent contacts in their extracellular domains. J. Gen. Physiol. 131:589–603. http://dx.doi.org/10.1085/jgp.200809976
- Yu, H., B. Burton, C.J. Huang, J. Worley, D. Cao, J.P. Johnson Jr., A. Urrutia, J. Joubran, S. Seepersaud, K. Sussky, et al. 2012. Ivacaftor potentiation of multiple CFTR channels with gating mutations. J. Cyst. Fibros. 11:237–245. http://dx.doi.org/10.1016/j.jcf.2011.12.005
- Zhang, J.Z., V. Yarov-Yarovoy, T. Scheuer, I. Karbat, L. Cohen, D. Gordon, M. Gurevitz, and W.A. Catterall. 2012. Mapping the interaction site for a β -scorpion toxin in the pore module of domain III of voltage-gated Na $^{+}$ channels. *J. Biol. Chem.* 287:30719–30728. http://dx.doi.org/10.1074/jbc.M112.370742
- Zhang, Z.R., G. Cui, X. Liu, B. Song, D.C. Dawson, and N.A. McCarty. 2005a. Determination of the functional unit of the cystic fibrosis transmembrane conductance regulator chloride channel. One polypeptide forms one pore. *J. Biol. Chem.* 280:458–468. http://dx.doi.org/10.1074/jbc.M409626200
- Zhang, Z.R., B. Song, and N.A. McCarty. 2005b. State-dependent chemical reactivity of an engineered cysteine reveals conformational changes in the outer vestibule of the cystic fibrosis transmembrane conductance regulator. *J. Biol. Chem.* 280:41997–42003. http://dx.doi.org/10.1074/jbc.M510242200
- Zhou, J.J., M. Fatehi, and P. Linsdell. 2008. Identification of positive charges situated at the outer mouth of the CFTR chloride channel pore. *Pflugers Arch.* 457:351–360. http://dx.doi.org/10.1007/s00424-008-0521-6